NAVAL POSTGRADUATE SCHOOL

Monterey, California

THESIS

EVALUATION OF SURFACE EXCHANGE COEFFICIENTS FROM MILDEX OCEAN/ATMOSPHERE MIXED LAYER DATA

by

Hardi S. Rosner

March 1985

Thesis Advisor: K. L. Davidson

Approved for public release; distribution is unlimited.

SECURITY CLASSIFICATION OF THIS PAGE (When Data Entered)

REPORT DOCUMENTATION PAGE		READ INSTRUCTIONS BEFORE COMPLETING FORM
1. REPORT NUMBER	2. GOVT ACCESSION NO.	3. RECIPIENT'S CATALOG NUMBER
4. TITLE (and Subtitle) Evaluation of Surface Exchange Coefficients from Ocean/Atmosphere Mixed Layer Data		5. TYPE OF REPORT & PERIOD COVERED Master's Thesis March 1985
		6. PERFORMING ORG. REPORT NUMBER
7. AUTHOR(s) HARDI S. ROSNER		8. CONTRACT OR GRANT NUMBER(s)
9. PERFORMING ORGANIZATION NAME AND ADDRESS Naval Postgraduate School Monterey, California 93943		10. PROGRAM ELEMENT, PROJECT, TASK AREA & WORK UNIT NUMBERS
11. CONTROLLING OFFICE NAME AND ADDRESS Naval Postgraduate School Monterey, California 93943		12. REPORT DATE March 1985
		13. NUMBER OF PAGES 74
14. MONITORING AGENCY NAME & ADDRESS(If different from Controlling Office)		15. SECURITY CLASS. (of this report) Unclassified
		15a. DECLASSIFICATION/ DOWNGRADING SCHEDULE

16. DISTRIBUTION STATEMENT (of this Report)

Approved for public release; distribution is unlimited.

17. DISTRIBUTION STATEMENT (of the abstract entered in Block 20, if different from Report)

18. SUPPLEMENTARY NOTES

19. KEY WORDS (Continue on reverse side if necessary and identify by block number)

Marine Atmospheric Boundary Layer; Oceanic Boundary Layer; Coupled Boundary Layer Model; interface; well-mixed layers; surface turbulent fluxes; friction velocity; MILDEX

20. ABSTRACT (Continue on reverse side if necessary and identify by block number)

A coupled oceanic-atmospheric boundary layer model which provides single-station prediction capability is evaluated relative to wind stress and oceanic mixed layer depth observations. The model is initialized and verified using data obtained during the 1983 Mixed Layer Dynamics Experiment (MILDEX). Model computation of friction velocity (u*) and oceanic mixed layer depth are compared with observations from both atmospheric frontal and

DD FORM 1 JAN 73 1473 EDITION OF 1 NOV 65 IS OBSOLETE

S/N 0102-LF-014-6601

non-frontal synoptic situations. Favorable results of model u* predictions are achieved although in some cases they are slightly higher than observed turbulence derived values of u*. Mixed layer predictions are very close to the observed except in frontal regions. Proper ABL/OBL model initialization of boundary layer values is critical in order to achieve favorable results.

Approved for public release; distribution is unlimited.

Evaluation of Surface Exchange Coefficients from MILDEX Ocean/Atmosphere Mixed Layer Data

by

Hardi S. Rosner
Lieutenant, United States Navy
B.A., Eastern College, 1973
M.S., University of Southern California, 1982

Submitted in partial fulfillment of the
requirements for the degree of

MASTER OF SCIENCE IN METEOROLOGY AND OCEANOGRAPHY

from the

NAVAL POSTGRADUATE SCHOOL
March 1985

ABSTRACT

A coupled oceanic-atmospheric boundary layer model which provides single-station prediction capability is evaluated relative to wind stress and oceanic mixed layer depth observations. The model is initialized and verified using data obtained during the 1983 Mixed Layer Dynamics Experiment (MILDEX). Model computation of friction velocity (u*) and oceanic mixed layer depth are compared with observations from both atmospheric frontal and non-frontal synoptic situations. Favorable results of model u* predictions are achieved although in some cases they are slightly higher than observed turbulence derived values of u*. Mixed layer predictions are very close to the observed except in frontal regions. Proper ABL/OBL model initialization of boundary layer values is critical in order to achieve favorable results.

TABLE OF CONTENTS

LIST OF TABLES

LIST OF FIGURES

ACKNOWLEDGEMENTS

I wish to thank:

- Professor K.L. Davidson for his continuous guidance and encouragement;
- Professor R.W. Garwood for his review of the thesis and constructive criticism;
- Dr. G.L. Geernaert for giving me the initial interest in the thesis subject matter and guiding me through its development;
- Ms. P. Boyle for patiently correcting my programming SNAFU's and her enormous assistance in data acquisition;
- Ms. S. Fellbaum for diligently retrieving and processing MILDEX data;
- Mr. T. Stanton for his assistance in retrieving CTD data; and
- Scripps Institute of Oceanography for providing ocean data from the R/P FLIP.

Very special thanks are reserved for Deborah, Kristin, Benjamin and Timothy for their unbounded patience, understanding, love and support over the last two and one-half years.

I. INTRODUCTION

Naval oceanographers and meterologists obtain a great variety of information to help them in making atmospheric and oceanic forecasts. Extensive use of large shore based computers, remote sensing equipment and world-wide communications networks make the forecaster rely on remotely based technology rather than local indicators and have, to a great degree, removed the "art" from single-station forecasting.

However, large-scale conflict or operational considerations could deny all forecasting inputs available to the forecaster except local indications. Reliance on single-station forecasting for naval operations during times of crisis or war was first addressed by Oliver and Oliver (1945):

> During the last few years, wartime conditions have made it necessary for isolated combat units to issue forecasts in regions where no network of meteorological stations could be available. Frequently the data from several stations or from reconnaissance planes are available, but in some regions the forecaster must rely only on surface and upper-air observations made at his own station. This is particularly true in the case of ships at sea. Hence, it is important to develop proficiency in extracting information from limited aerological data.

While the above quote pertains to atmospheric forecasts, the same could be true for ocean predictions.

In modern warfare, isolated ships or battle groups far from the main force, operating in an emission control (EMCON) posture, must be able to predict their operating environment without shore support. Such predictions are important for the effective utilization of weapon and sensor systems and to deny the effective use of the environment to the opposing force. Affected systems include: navigation

radars, communications equipment, over-the-horizon (OTH) radars, air and surface search radars, missile and gun fire control radars, laser and infra-red (IR) guided missiles, hull mounted sonars, towed arrays, and variable depth sonars (VDS).

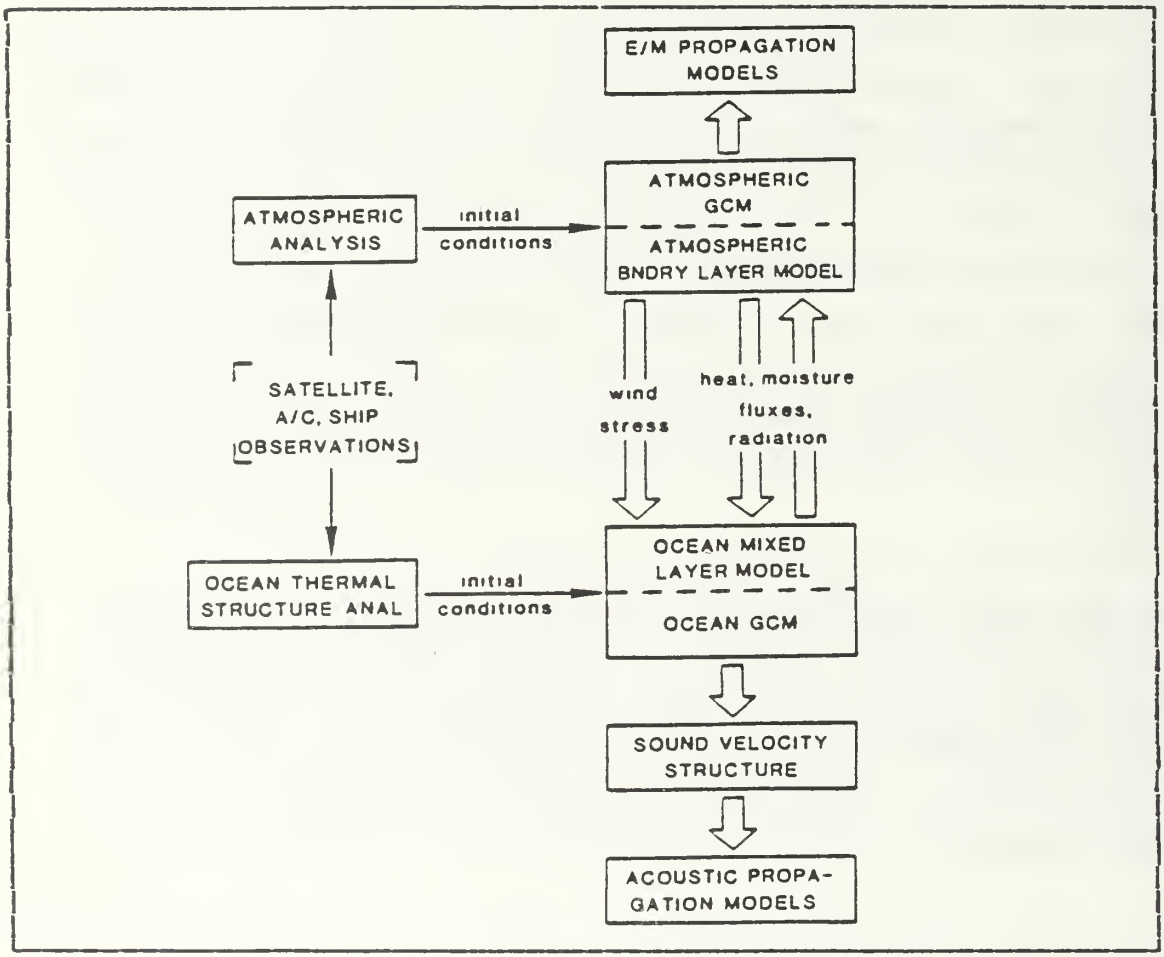

Fig. 1.1 Components of the Coupled Atmospheric and Oceanic Boundary Layer Model.

A coupled atmospheric and oceanic model (O'Loughlin, 1982) has been developed to predict ocean and atmospheric parameters from local indications. The components of this coupled model are depicted in Fig. 1.1. This model is being

tested and evaluated with shipboard applications in mind. Accurate predictions of ocean mixed layer depths (MLD), thermocline jumps and gradients are essential in optimizing anti-submarine warfare (ASW) systems and employing acoustic countermeasures. These parameters are dependent on the heat fluxes and wind stress at the ccean surface. This thesis will examine how the single-station coupled model predicticns of the surface fluxes and mixed layer depth compare with observations.

II. MODEL BACKGROUND AND ANALYSIS PROCEDURES

A. BOUNDARY LAYER DESCRIPTION

Thermodynamically and dynamically forced marine atmospheric (MABL) and oceanic (OBI) boundary layers must be considered in coupled model description. The air-sea interface has adjacent oceanic and atmospheric turbulent mixed layers which effectively insulate the quasi-geostrophic oceanic and atmospheric flows above the top of the MABL and below the bottom of the OBL. The primary source of the turbulence is the velocity (shear) and buoyancy (density) gradients created by the exchange of mass, energy and momentum across the air-sea interface. Such turbulence generates turbulent kinetic energy (TKE) and vigorous vertical mixing (Davidson and Garwood, 1984).

Under undisturbed conditions, the MABL consists of a moist, well-mixed layer extending from the surface to the capping inversion. At the inversion, jumps in temperature and humidity occur with a rapid increase in temperature and a corresponding decrease in humidity. Within the MABL, equivalent potential temperature and specific humidity are conservative quantities.

A consequence of the large velocity fluctuations and mixing in the MABL is that energetic eddies (extending from the surface to the inversion) entrain warm, dry air and bring momentum into the mixed layer. This results in the upward growth of the layer. Subsidence arises from large-scale atmospheric forcing and tends to limit the depth of the mixed layer. Therefore, the change in the inversion height with respect to time is a function of the entrainment rate and subsidence. If entrainment causes the MABI to

extend above the lifting condensation level (LCL), clouds or fog will form within the layer and greatly affect the OBL.

In the ocean, the OBL is defined as extending from the surface to the top of the seasonal thermocline. Within the mixed layer, nearly homogeneous profiles of temperature and density are evident. While density is a function of both salinity and temperature, over short time scales, temperature has a far greater effect (Miller, 1976). At the bottom of the mixed layer, large changes in temperature and salinity exist with increasing depth. This is the top of the thermocline region and serves as a transition from the mixed layer to the usually dynamically stable interior ocean. Idealized model profiles for both the MABL and OBL are depicted in Fig. 2.1.

Radiation is another source of energy in both mixed layers. While most solar energy will penetrate the MABL, this is not true of the OBL. Long wave radiation is absorbed and emitted by the first few millimeters of sea water. Therefore downward turbulent heat flux is as important as the upward flux. Surface heat flux in the OBL is a function of sensible and latent heat as well as the long and short wave solar radiation. This radiation is highly dependent on cloud formation in the ABL so proper ABL modelling is essential for realistic ocean MLD predictions.

While buoyancy forces create turbulence in both boundary layers, relatively more turbulence in the OBL is produced by wind stress (Davidson and Garwood, 1984). The MLD will deepen if the wind generated downward flux of momentum and forced convective mixing (of surface water that has been cooled by radiative heat loss or evaporation) provide sufficient TKE to erode the thermocline and entrain cooler water downward. If, on the other hand, the near surface absorption of solar radiation produces a downward buoyancy flux which dampens turbulence and provides for net warming, the

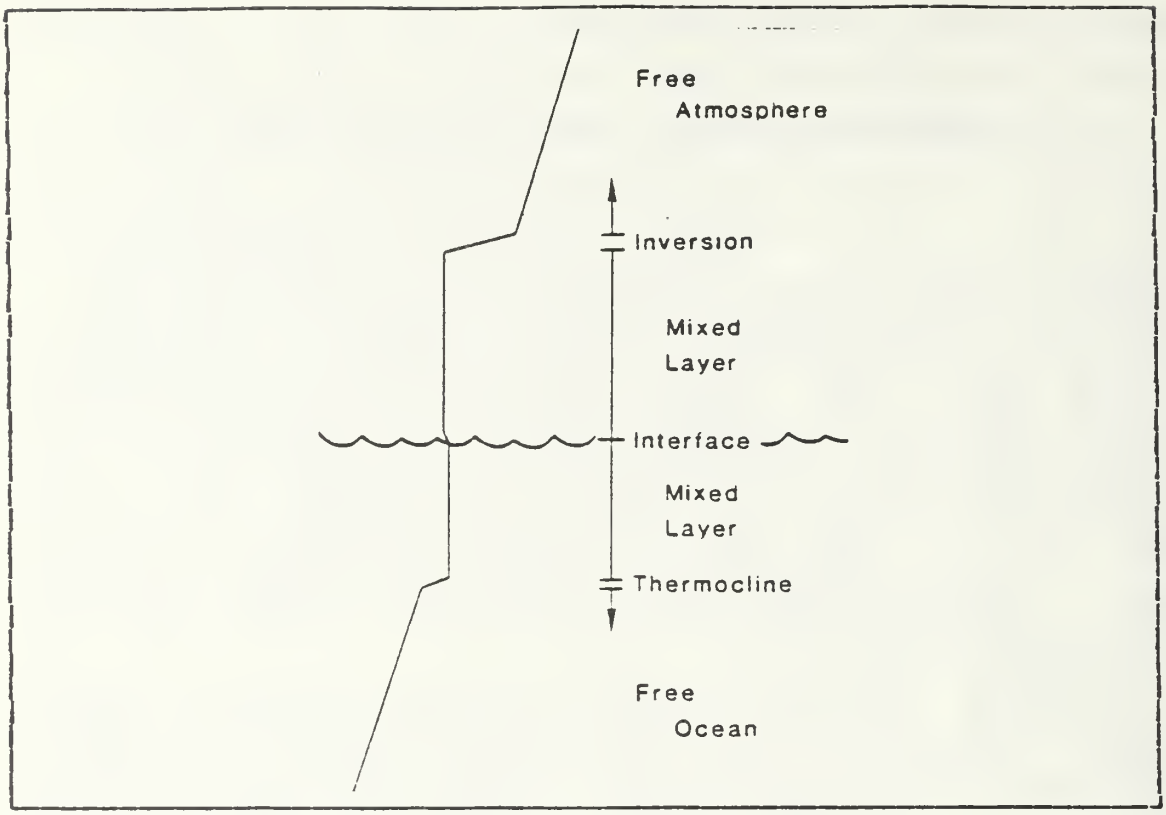

Fig. 2.1 Idealized Atmospheric and Oceanic Boundary Layer Temperature Profile.

MLD will shallow. Fig. 2.2 shows the importance of mechanical mixing to the CBL and its interaction with buoyancy fluxes. A primary objective of this thesis will be to determine the effects of wind stress on the MLD.

Several cause and effect relationships are evident. First, clouds can be caused by changes in the ocean surface temperatures which, in turn, affect the radiation budget of the OBL which results in surface temperature changes. Secondly, the stability of the MABL is influenced by air-ocean temperature differences. Again, cloud formation plays an important role. Such relationships make a coupled prediction approach necessary. This coupled model uses local oceanic descriptions from a bulk oceanic mixed layer

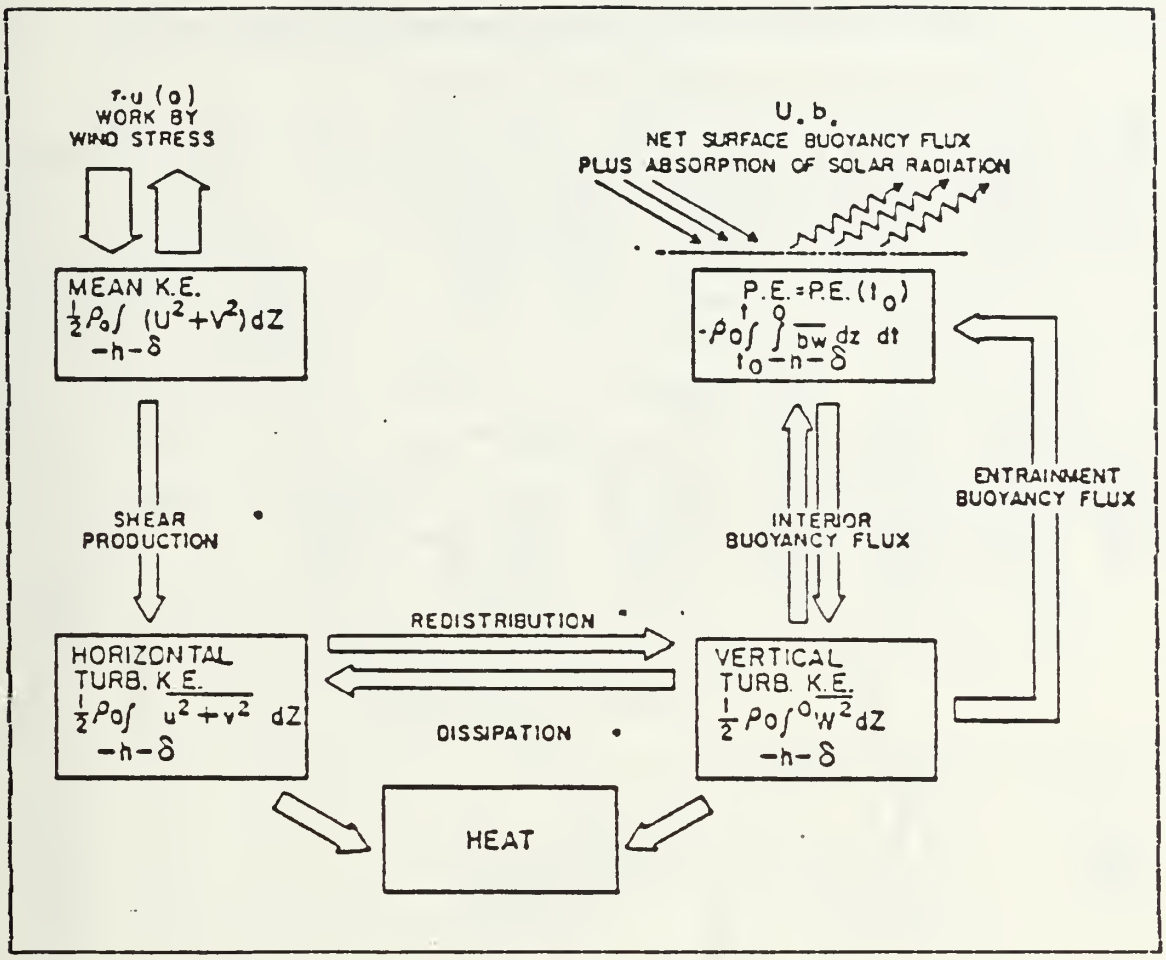

Fig. 2.2 Mechanical Energy Budget for the Ocean Mixed Layer.

model and the atmospheric descriptions come from an atmospheric boundary layer model. Such a coupled model has tactically significant implications to forecast parameters that are important to weapons systems. Fig. 2.3 shows the interrelationships between the coupled model and tactical products which can use model outputs (on the extreme right hand side).

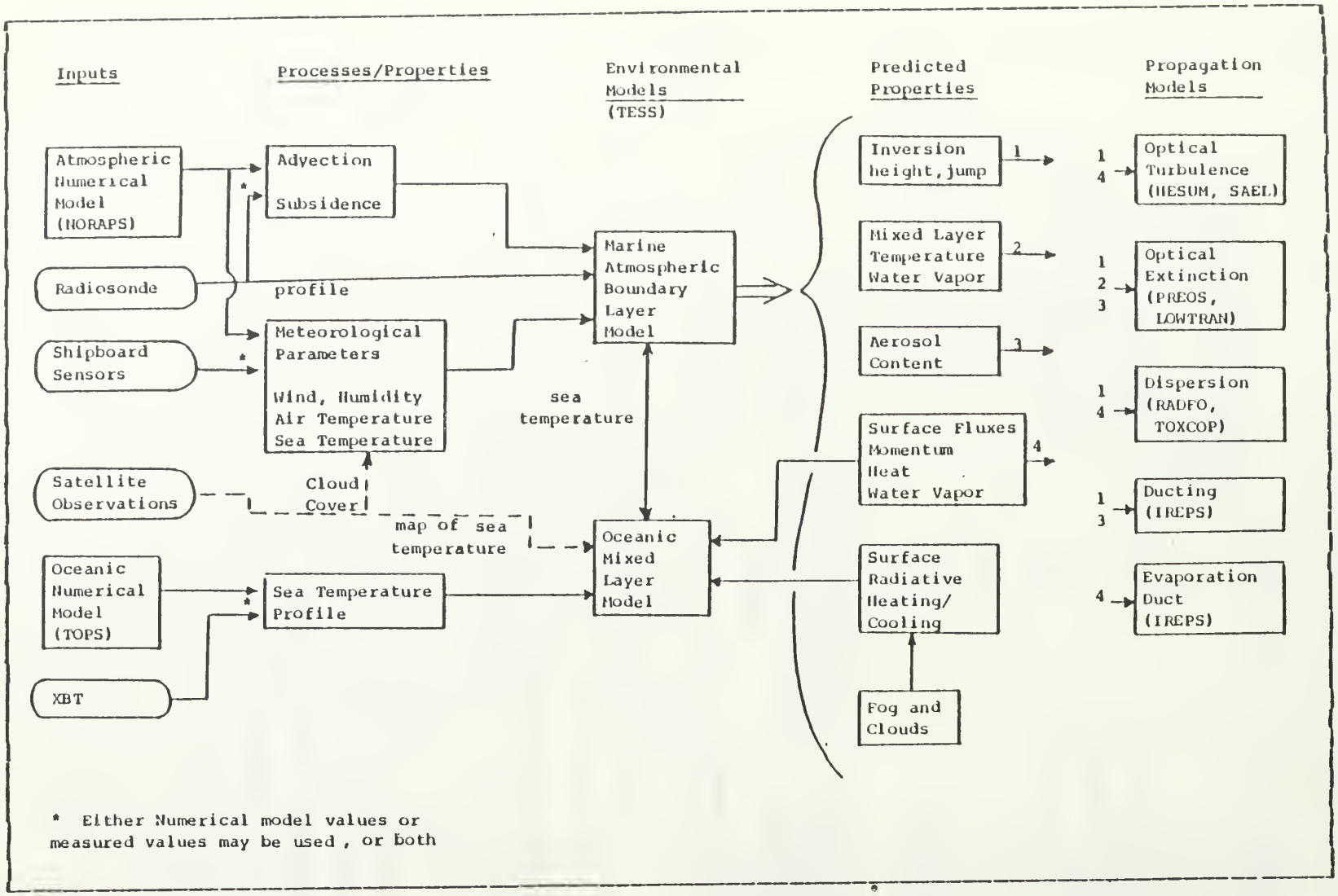

Fig. 2.3 Flow Diagram of a Coupled Model, Outputs and Tactical Utilization.

B. MARINE ATMOSPHERIC BOUNDARY LAYER (MABL) MODEL

Existing integrated MABL models are zero-order, two layer, mixed layer models consisting of a well mixed turbulent boundary layer underneath a relatively non-turbulent free atmosphere. A transition zone (inversion) of zero thickness (hence the term zero-order) separates the two layers. Because it has no thickness, a jump occurs at the inversion of the conservative parameters. The model was described by Stage and Businger (1981), who formulated entrainment energetics, and modified by Davidson, et al. (1984), who described bulk aerodynamic formulae for the surface layer.

The following inputs are required by the model:

(1) an initial atmospheric sounding;

(2) the mean winds at a level within the surface layer;

(3) the surface temperature; and

(4) the subsidence rate.

As formulated, ten winds can be input over the forecast period. The sea-surface temperature (SST) remains unchanged and the surface current is assumed to be zero. SST and the surface current change in the coupled version due to the interaction with the OBL model. Inversion height, mixed layer values of temperature, humidity and wind are predicted at 30-minute intervals in both the coupled and uncoupled versions. The prediction steps are shown in Fig. 2.4. Procedures are the same for clear and cloudy cases except for entrainment computation and estimation of cloud top cooling. Formation of clouds or fog, cloud top cooling and associated entrainment are important in the physical processes in the MABL.

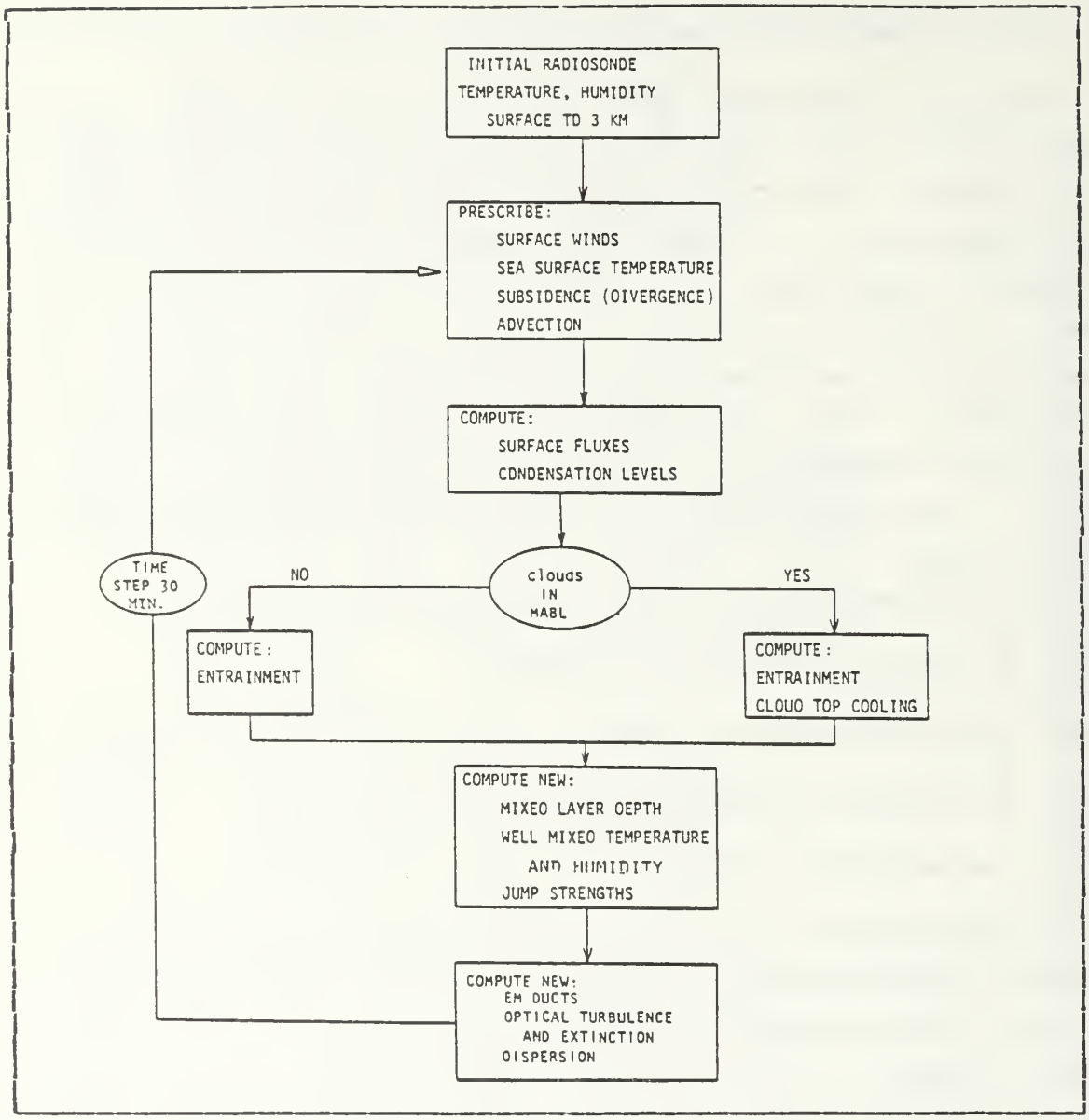

Fig. 2.4 Schematic of Input, Prescription and Computing Steps in MABL Prediction.

The MABL model is very sensitive to the prescribed large scale subsidence which moderates the depth of the moist marine layer and hence, cloud formation. Methods which can be used to compute the subsidence from single station observations are: the kinematic method; the adiabatic method;

and the integration of the moisture budget equation (Q) method. Gleason (1982) found that the Q-method has the most merit and was used in this thesis. However, this method assumes that no advection will take place.

Integrated rate equations by Tennekes and Dreidonks (1981) are used to predict the time rate of change of the conservative quantities and their respective jumps at the inversion. The vertically integrated equations for a conserved property, X, are:

$$h(DX/Dt) = (\overline{w'x'})_o - (\overline{w'x'})_h + \text{source} \qquad (2.1)$$

$$h(D\Delta X/Dt) = h\Gamma x(\partial h/\partial t) - (\overline{w'x'})_o + (\overline{w'x'})_h - \text{source} \qquad (2.2)$$

where:

$\text{source} = -(F_{nh} - F_{no})/\rho C_p$ for X = temperature

source = 0 for X = humidity

and Gamma (Γ) is the conservative property lapse rate above the inversion and F_n is the net radiative flux. The subscripts "h" and "o" refer to inversion height and surface values respectively.

The entrainment velocity parameterization is based on the formulation by Stage and Businger (1981) and is used to close the system of equations and determine the time evolution of the inversion height. The closure assumpton is that the dissipation rate of the TKE is a fixed fraction (1-A) of the production rate. "A" is the entrainment coefficient and is taken to be 0.2.

Bulk aerodynamic formulas described by Davidson, et al. (1984), are used to determine the surface fluxes of momentum, sensible heat and latent heat. They are:

$$u^* = C_d^{1/2} U_{10} \qquad \text{(friction velocity)} \qquad (2.3)$$

$$T^* = C_\theta^{1/2}(\theta_o - \theta) \quad \text{(temperature parameter)} \tag{2.4}$$

$$q^* = C_\theta^{1/2}(q_o - q) \quad \text{(moisture parameter)} \tag{2.5}$$

These fluxes are given by:

$$\overline{u'w'} = u^{*2} \quad \text{(momentum)} \tag{2.6}$$

$$\overline{T'w'} = u^*T^* \quad \text{(sensible heat)} \tag{2.7}$$

$$\overline{q'w'} = u^*q^* \quad \text{(latent heat)} \tag{2.8}$$

where C_d and C_θ are the stability dependent wind and temperature drag coefficients, θ is the potential temperature and q is the specific humidity. The subscript "o" denotes the surface value.

Because radiation is a primary factor in the OBL development, considerable effort has gone into calculating the radiation budget in the MABL. Uncertainty in background aerosols, distribution and concentration of atmospheric absorbing gases, and cloud droplet size spectra are sources of error in the MABL radiation calculations. The short and long wave fluxes are computed separately. Short wave radiative flux is calculated using the delta-Eddington method (Joseph, et al.,1976) which accounts for heating of the mixed layer by solar radiation. Incident flux at the top of the mixed layer is obtained from the flux at the top of the atmosphere and the average transmittance in each of 15 bands covering the spectrum from 0.2 um to 1.7um. Short wave extinction is due to both scattering and absorption. Water vapor in the atmosphere is the primary absorbing constituent. Scattered radiation forms a second short wave radiative component (diffuse solar radiation) which, in the mixed layer, is due to atmospheric particles (cloud droplets and

aerosols). Total short wave radiative flux at the surface is determined by computing both the direct and diffuse radiative components. Fairall, et al. (1981) gives a comprehensive review of this method. Solar zenith angle is necessary in order to compute short wave radiative flux and it is determined from the latitude, julian day and time of day of the initial input. The fraction of short wave radiation from the sea surface, Ag, which is an important short wave ratiative parameter, is prescribed in the MABL model as 0.1.

Long wave radiative flux is calculated differently for the cloudy and cloud free cases. In the cloudy case, the only clouds permitted are non-black stratus. Radiative flux is a function of cloud emissivity, ϵ_c, which depends on the total liquid water content, W, of the cloud. W profiles are nearly linear with height above the LCL (Davidson, et al., 1984) and, along with ϵ_c can be described by:

$$W = 0.5 \rho_a (h - Z_c) q_{lh} \tag{2.9}$$

$$\epsilon_c = 1 - \exp(-aW) \tag{2.10}$$

where ρ_a is the density of air (1.25×10^{-3} gm/cm^3), h is the height of the mixed layer (cloud top), Z_c is the LCL (cloud bottom), a = 0.158 (Slingo, et al., 1982), and q_{lh} is the liquid water content at the cloud top.

Using the Stefan-Boltzmann law, the net long wave cloud top radiation flux, L_{nh}, can be calculated from the cloud top temperature, T_h, and the effective radiative sky temperature, T_{sky}, cloud bottom net radiative flux, L_{nc}, is calculated in the same way using the cloud bottom temperature, T_c, and the SST, T_s. These fluxes are given by:

$$L_{nh} = \epsilon_c \sigma (T_h^4 - T_{sky}^4) \tag{2.11}$$

$$L_{nc} = \epsilon_c \sigma (T_s^4 - T_c^4) \tag{2.12}$$

where σ is Stefan's constant (4.61×10^{-11}) and ϵ_c is obtained from equation 2.10 . The net long wave flux at the surface, F_{long}, becomes:

$$F_{long} = \sigma [T_s^4 - \epsilon_c \overline{T}^4 - (1 - \epsilon_c) T_{sky}^4] \qquad (2.13)$$

where $\overline{T}$ is the average temperature of the cloud.

For the cloud free case, the net fluxes are calculated at the top of the mixed layer (Z = h) and at the surface (Z = 0) by integrating the flux emissivity profile (Fleagle and Businger, 1980), which is a function of the water vapor and temperature profiles. The net long wave flux at the surface for the clear sky case is:

$$F_{long} = F_u - F_d \qquad (2.14)$$

where F_u and F_d are the upward and downward radiative fluxes respectively.

C. OCEANIC BOUNDARY LAYER (OBL) MODEL

The OBL model is a one-dimensional, second order turbulence closure, vertically integrated (bulk) model of the upper ocean surface turbulent boundary layer or mixed layer developed by Garwood (1977). It uses the continuity equation for an incompressible fluid, the first law of thermodynamics (heat equation), the conservation of salt equation, an analytical equation of state, the Navier-Stokes equation of motion with the geostrophic component eliminated, and a two-component vertically integrated TKE budget.

An understanding of the dynamics of the entrainment process is necessary to predict the MLD change with time. The stable water mass underneath the mixed layer is destabilized and eroded by TKE in the mixed layer. This TKE budget

is the basis for an entrainment hypothesis. A closed system of equations is obtained by using the bulk buoyancy and momentum equations with the mean turbulent field modeling of the vertically integrated equations for the individual TKE components.

To better define the mixing process, separate vertical and horizontal equations for TKE are used. Buoyancy flux and shear production provide energy for vertical mixing, with buoyancy flux being a somewhat more efficient source of energy for mixing due to its direct contribution to the vertical component of TKE. The buoyancy equation is derived from the heat and salt equations using a linearized equation of state:

$$\overline{\rho} = \rho_o[\, 1 - \alpha(\widetilde{\vartheta} - \vartheta_o) - \beta(\widetilde{S} - S_o)\,] \qquad (2.15)$$

Buoyancy is given by:

$$\widetilde{b} = g(\rho_o - \widetilde{\rho})/\rho_o \qquad (2.16)$$

where:

ϑ = temperature

S = salinity

g = gravity

ρ = density

α = thermal expansion coefficient

β = density coefficient for salt

The tilde represents the total instantaneous value and the subscript "o" denotes an arbitrary, but representative, constant value. In the short term, salinity has little

effect on the upper ocean density profile except at higher latitiudes (Miller, 1976). This leaves temperature as the dominant density factor. However, by using buoyancy (b) instead of only temperature (θ) allows the model to be applied in cases where evaporation and/or precipitation contribute significantly to the surface buoyancy flux.

Model initialization requires:

(1) mixed layer temperature and salinity profiles;

(2) wind-driven horizontal current profiles.

The initial salinity profile is made isohaline if unknown and the initial currents are assumed to be zero if unknown. Lack of initial information about current and salinity profiles is not a serious deficiency because the model will evolve reasonable transient profiles of salinity and momentum after only a single diurnal cycle, and the final results are not sensitive to the initial current and salinity profiles (Davidson and Garwood, 1984). It is also possible to prescribe an upper ocean internal vertical velocity (upwelling and downwelling) if it is known to be significant. The mixed layer depth, h, is defined as the shallowest depth at which the observed density value, σ_t, is 0.02 σ_t units greater than the observed surface density value.

At each one hour model time step, the following boundary conditions are required:

- net upward turbulent heat flux at the water surface (sensible and latent heat flux) plus back radiation;
- incident solar radiation;
- the fraction of short wave radiation absorbed in the top one meter of the ocean;
- surface wind speed and direction;

- cloud cover;
- temperature (SST, dry bulb and dew-point air temperature); and
- precipitation (P).

Vertical velocity at the bottom of the mixed layer may be prescribed hourly. Other physical and model constants that need to be prescribed are:

- the extinction coefficient for short wave radiation absorption;
- the Coriolis parameter;
- the critical Richardson number for stability adjustment below the mixed layer;
- expansion coefficient for temperature; and
- density coefficient for salt.

The model forecast is not particularly sensitive to these constants, but reasonable values have been determined by Gallacher, et al. (1983), and they need not be readjusted for geographic and seasonal variability.

By use of bulk aerodynamic formulas, the turbulent fluxes of latent heat, Q_e, and sensible heat, Q_h, can be estimated as follows:

$$Q_e = C_d (.98E_s - E_a) U_{10} \qquad (2.17)$$

$$Q_h = C_d (T_s - T_a) U_{10} \qquad (2.18)$$

Net back radiation is estimated from the empirical equation (Husby and Seckel, 1978):

$$Q_b = 1.14 \times 10^{-7}(273.16 + T_s)^4(.39 - .5E_a^{1/2})(1 - .6C^2) \quad (2.19)$$

where:

E_s = saturated vapor pressure of the marine air (0.98 corrects for salt defects)

E_a = vapor pressure of air based on dew point temperature

T_a = air temperature

T_s = sea surface temperature

C = fractional cloud cover

C_d = drag coefficient

The upward heat flux, Q_u, is then given as:

$$Q_u = Q_e + Q_h + Q_b \quad (2.20)$$

and the solar radiation, Q_s, by:

$$Q_s = (1 - a\alpha^b)(1 - .66C^3)Q_o \quad (2.21)$$

The constants "a" and "b" are adapted from Tabata (1964) and the cubic cloud cover correction from Laevastu (1960). Clear sky radiation, Q_o, is given by Seckel and Beaudry (1973):

$$Q_o = A_o + A_1 \cos \phi + B_1 \sin \phi + A_2 \cos 2\phi + B_2 \sin 2\phi \quad (2.22)$$

where the coefficients (A_o, A_1, etc.) were calculated by harmonic representation of the values predicted in the

Smithsonian Meteorological Tables (List 1958) with:

$$\phi = (2\pi/365)(t - 21) \tag{2.23}$$

where "t" is the julian day of the year.

The ocean is not very transparent to solar radiation. In the open ocean, approximately 50% is absorbed within the first meter (this fraction is called "Rf"). Absorption varies from region to region and is highly dependent on the concentration of absorbing particles such as phytoplankton, "Gelbstoff" (yellow substance), and suspended particulate matter. Coastal regions absorb more radiation because of increased amounts of suspended particulates. Very little of this absorbed radiation penetrates below the mixed layer because of the low thermal conductivity of the underlying stable thermocline. Thus most of this energy is transferred upward out of the ocean and back into the atmosphere. What short wave radiation remains penetrates the mixed layer and is attenuated in an exponential fashion depending on water turbidity. Net heat flux at the surface is given as:

$$Q_{net} = Q_u + (Rf)Q_s - Q_s \tag{2.24}$$

Surface buoyancy (heat and salt) and momentum fluxes can be computed by use of the foregoing equations. Mixed layer turbulent temperature, salinity, velocity and buoyancy fluxes are given by:

$$(\overline{T'w'}) = -Q_{net}/\rho C_p \tag{2.25}$$

$$(\overline{S'w'}) = (P - E)S_o \tag{2.26}$$

$$(\overline{u'w'}) = u^{*2} \tag{2.27}$$

$$(\overline{b'w'}) = g[\alpha(\overline{T'w'}) - \beta(\overline{S'w'})] \tag{2.28}$$

where the subscript "o" refers to the surface value. The friction velocity in air, u*, is calculated by:

$$\tau_s = \rho_a C_d U_{10}^2 \qquad (2.29)$$

$$u^* = (\tau_s / \rho_a)^{1/2} \qquad (2.30)$$

where τ_s is the surface stress (dynes/cm^2). The fluxes of momentum, radiation, latent and sensible heat at the sea surface determine shallowing (retreat) or deepening of the mixed layer by entrainment. If there is a positive buoyancy flux ($Q_{net}<0$ and $E>P$) the MLD will deepen. This will be the case at night or whenever long wave radiative cooling plus the upward turbulent fluxes of heat and moisture exceed solar radiation. Negative buoyancy flux will result in the shallowing of the MLD and is caused by the domination of daytime solar heating (net warming) at the surface, provided wind stress is not large.

A schematic of the ocean model computations is shown in Fig. 2.5. New ocean temperature, salinity and wind-driven current profiles are predicted at one-hour intervals and are used to predict the new MLD.

D. COUPLED BOUNDARY LAYER MODEL

Coupling of the atmospheric and oceanic models was first accomplished by O'Loughlin (1982) by matching momentum, sensible heat, latent heat, and radiation at the air-sea interface. The atmospheric part of the coupled model computes the radiative, heat and momentum fluxes which are inputs to the ocean model. Since the ocean model has an hour time step, and the atmospheric model has a half-hour time step, the ocean model was inserted as a subroutine into the atmospheric model and is called every other atmospheric

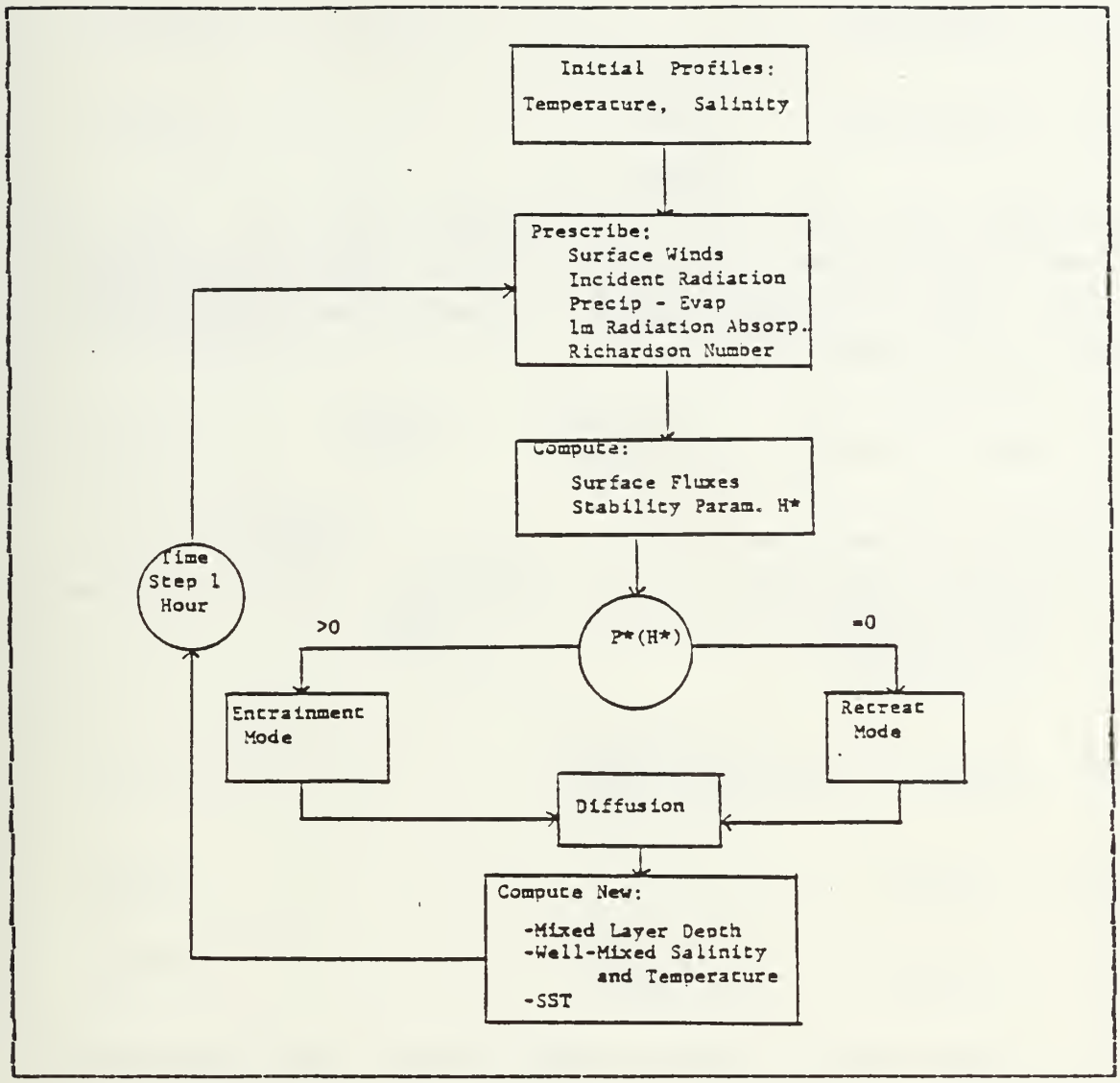

Fig. 2.5 Schematic of Input, Prescription and Computing Steps in OBL Prediction.

time step. Before the atmospheric fluxes can be utilized by the ocean model, they must be converted to the appropriate units for seawater.

The ocean model prediction requires the vector surface stress for the ocean turbulent velocity flux, $u^*_w{}^2$. This requires that the wind field be broken into horizontal components:

$$U_{10x} = -(\sin \theta) U_{10} \tag{2.31}$$

$$U_{10y} = -(\cos \theta) U_{10} \tag{2.32}$$

where U_{10} is the wind speed at 10 meters and U_{10x}, U_{10y} are the east-west and north-south horizontal components respectively. The wind direction, θ, is relative to true north. Then $u*_w{}^2$ is given by:

$$\tau_s = \rho_a u*^2 = \rho_w u*_w{}^2 \tag{2.33}$$

the density of seawater, ρ_w, to be about 1 gm/cm^3. Finally, the horizontal components of the turbulent velocity fluxes, $u*_{wx}{}^2$ and $u*_{wy}{}^2$, are computed by:

$$u*^2 = C_\theta U_{10}{}^2 = C_\theta (U_{10x}{}^2 + U_{10y}{}^2) \tag{2.34}$$

$$u*_{wx}{}^2 = C_\theta U_{10x}{}^2 \tag{2.35}$$

$$u*_{wy}{}^2 = C_\theta U_{10y}{}^2 \tag{2.36}$$

SST is passed from the MABL model back to the atmospheric model for use in the next time step. Fig. 2.6 shows the interrelationships between the atmospheric and oceanic models in the coupled model.

The coupling process has the potential of significantly enhancing the OBL prediction qualities because of the improvement in the boundary conditions inherent in a coupled OBL-MABL system. Longer period reasonable forecasts should be obtained due to the feedback between the adjacent turbulent boundary layers and the associated thermodynamic and dynamic adjustments in each layer. Formation of stratus or fog in the MABL model is particularly important. Accurately

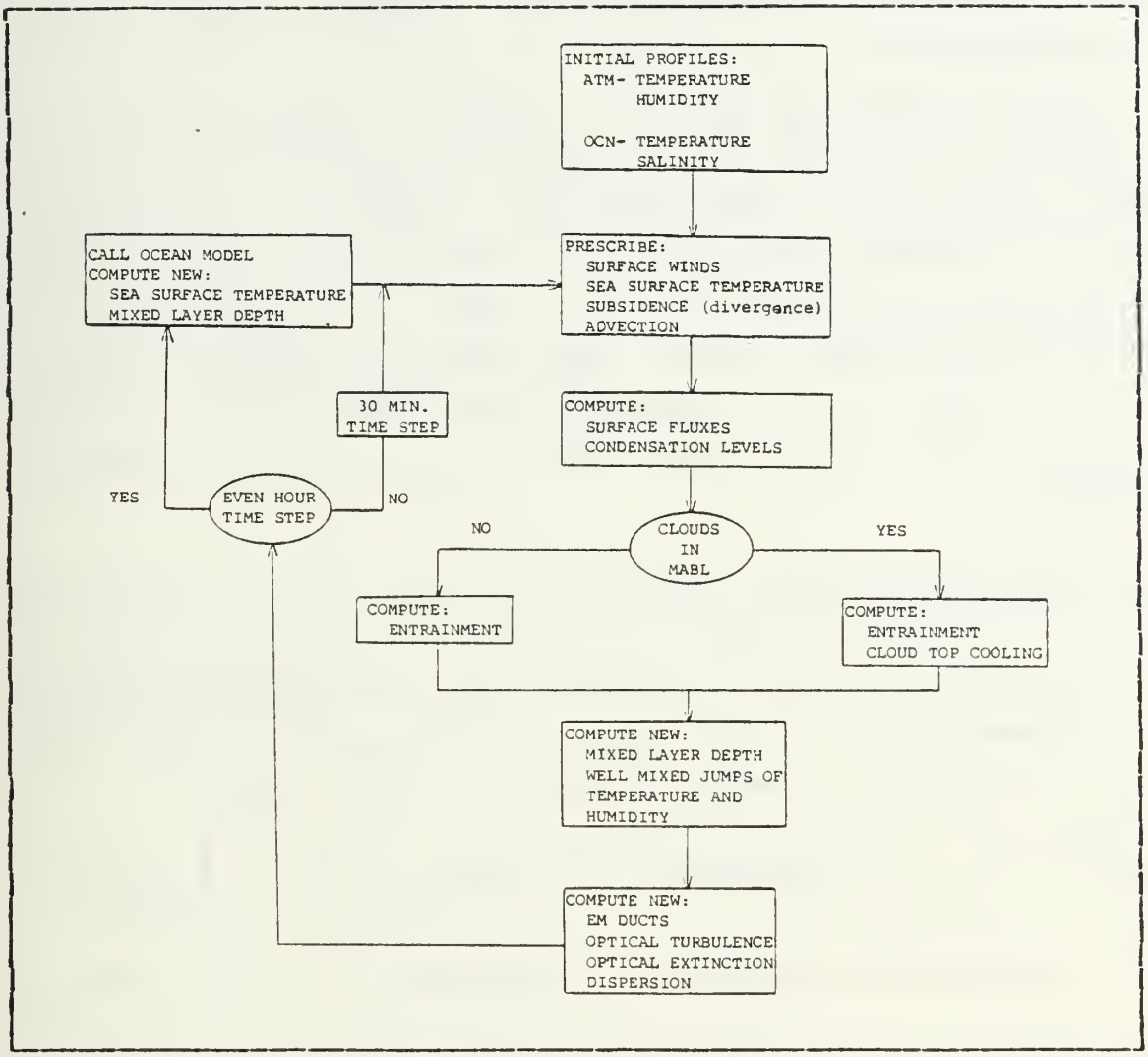

Fig. 2.6 Flow Chart for Ccupled OBL and MABL Model

prescribed incoming solar radiation is imperitave for a useable OBL forecast. This can only be done by use of an MABL model such as has been described in section B (Davidson and Garwood, 1984).

E. U* ESTIMATION FROM TURBULENT KINETIC ENERGY (TKE) DISSIPATION

Direct measurement of u* on a ship is rather difficult. One popular technique which is used extensively at the Naval Postgraduate School is the dissipation method. An excellent review of this method as well as the bulk method is contained in Schacher, et al. (1981). The dissipation method involves the use of the turbulent kinetic energy (TKE) equation which, assuming steady conditions and the divergence term to be small relative to the other terms, becomes:

$$u^* = \{[\epsilon kz]/[\phi_m(z/L) - (z/L)]\}^{1/3} \qquad (2.37)$$

The denominator on the right hand side of equation 2.37 has been parameterized, where the quantity $\phi_m(z/L) - (z/L)$ is substituted by ϕ_ϵ following Wyngaard and Cote (1971):

$$\phi_\epsilon = (1 + 0.5\ |z/L|^{3/5})^{3/2} \qquad \text{for } z/L < 0 \qquad (2.38)$$

$$\phi_\epsilon = (1 + 2.5\ (z/L)^{2/3})^{3/2} \qquad \text{for } z/L > 0 \qquad (2.39)$$

Determination of the dissipation rate, ϵ, necessary for this technique requires that the inertial subrange follows a Kolmogorov spectrum, i.e., where:

$$S_u(k^*) = \alpha\, \epsilon^{2/3} k^{*-5/3} \qquad (2.40)$$

$S_u(k^*)$ in equation 2.40 is the spectral density of the horizontal windspeed, α is a coefficient with a magnitude of 0.52 (Champagne, et al., 1977), and k^* is the wavenumber. Equation 2.40 has been experimentally verified. On the R/V Acania a hot film sensor was used to obtain a spectrum of

high frequency velocity fluctuations from which the TKE dissipation u* was calculated. It is important to note here that poor velocity turbulence spectra are obtained during periods of fog, rain or drizzle. This leads to the dissipation method being invalid. Errors may also occur if the relative wind is less than 3 m/s allowing condensation to form on the hot film.

Applying Taylor's hypothesis, i.e., $k^* = 2\pi f/\bar{U}$, equation 2.40 may be rearranged to become:

$$\epsilon = 240\,[S_u(f)]^{3/2}\,(f/\bar{U})^{5/2} \qquad (2.41)$$

where f is frequency measured in Hz. The inertial subrange spectral densities are integrated between two wavenumbers, k_ℓ and k_h respectively, in equation 2.40 following Khalsa and Bussinger (1977):

$$\sigma_{\Delta k}^2 = \int_{k_\ell}^{k_h} S_u(k)\,dk = (3/2)\,\alpha\,\epsilon^{2/3}(k_\ell^{-2/3} - k_h^{-2/3}) \qquad (2.42)$$

Applying Taylor's hypothesis, equation 2.42 now becomes:

$$\sigma_{\Delta f}^2 = 0.230\,(\epsilon\bar{U})^{2/3}(f_\ell^{-2/3} - f_h^{-2/3}) \qquad (2.43)$$

Rearranging equation 2.43 and combining with equations 2.37, 2.38 and 2.39, with a von Karman constant of 0.4, we obtain:

$$u^* = 2.81\,\sigma_{u_{\Delta f}}\{z/[\bar{U}\phi_\epsilon(z/L)]\}^{1/3}\{f_\ell^{-2/3} - f_h^{-2/3}\}^{1/2} \qquad (2.44)$$

Substituting f = 50Hz, f = 5Hz, the measurement height, z = 20.0m, equation 2.44 reduces to its operational form as follows:

$$u^* = 3.69\,\sigma_{u_{\Delta f}}[\bar{U}_{20m}\phi_\epsilon(z/L)]^{-1/3} \qquad (2.45)$$

Because z/L is a function of the friction velocity, u*, according to equations 2.38 and 2.39, the solution to equation 2.45 involves an iterative process (Large, 1979).

III. SYNOPTIC SITUATION

A. MIXED LAYER DYNAMICS EXPERIMENT (MILDEX)

The Mixed Layer Dynamics Experiment (MILDEX) was conducted during the period of 24 October to 10 November, 1983 near 34°N and 126°W. MILDEX was a multi-group and multi-platform experiment designed to:

- provide magnitudes of air-sea energy exchange rates for use as boundary conditions in mixed layer modelling.
- evaluate the drag coefficient from TKE dissipation measurements and its dependence on swell amplitude and direction.
- to provide a time series, from radiosonde measurements, of MABL structure for model verification.
- provide an intercomparison between radiative transfer algorithms developed at Scripps Institute of Oceanography and measured data.
- evaluate the utility of SODAR as a ship-borne instrument.
- evaluate radiative transfer models of the atmosphere with cloudiness as a unique parameter.

Meteorology data were collected on the R/V Acania as well as two other platforms during MILDEX. R/V Acania data collection consisted of measurements of windspeed, temperature, humidity, radiation and atmospheric pressure in the surface layer, and sea surface temperature (measured by thermistor), and radiosonde derived profiles of atmospheric windspeeds and directions, temperatures and humidity. Radiosonde launches were coordinated with satellite pass times.

Fig. 3.1 depicts the locations on the bow of the R/V Acania of mean and turbulent measurement sensors. There were two levels of these measurement sensors: bow mast at 5 meters and main mast at 20 meters. In addition, there were hourly observations of sea state and cloudiness. Conductivity, temperature and depth (CTD) casts were also made from the R/V Acania. Two other vessels, the R/V Wecoma and R/P FLIP collected meteorolcgical and oceanic data near the same site as R/V Acania. During the periods of interest in this thesis, the R/P FLIP was always within two kilometers of the R/V Acania. The meteorological data has been compiled in the MILDEX report (Geernaert, et al., 1983).

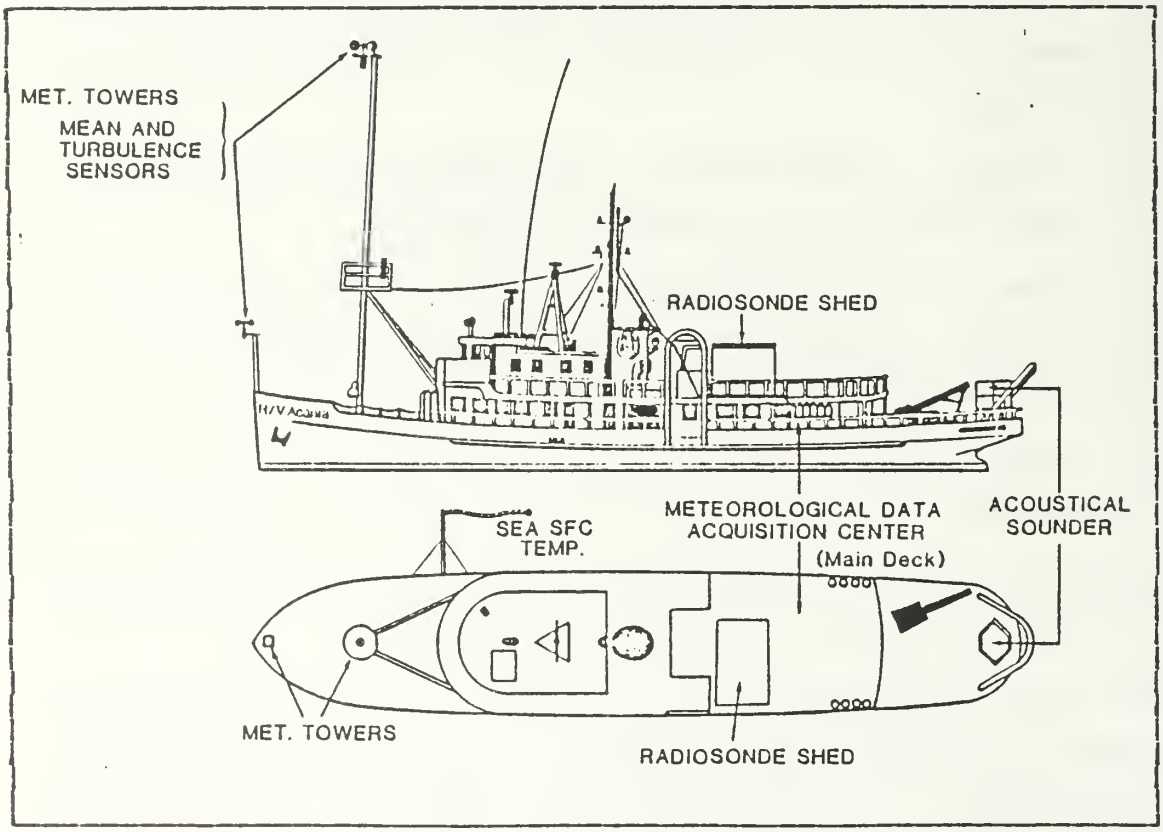

Fig. 3.1 Schematic of the R/V Acania

Time series of wind speeds, directions, SST, air temperature, and surface pressure in Fig. 3.2 show some of the variability experienced during MILDEX. Frontal passages are evident on 29 October, 31 October, and 06 November. For most of the experiment, the SST was greater than the air temperature (except on 29 October and 09 November), so the surface layer was unstable or near neutral. Only for 6-8 hour periods on 29 October and 09 November was the surface layer stable.

Three periods (cases) were considered for purposes of this study. These cases were chosen on the basis of strong wind forcing of the OBL and the availability of reliable radiosonde data for model initialization. Fig. 3.3 shows the movement of the R/V Acania for all three cases. The R/V Acania was located near 34.0N, 125.4W during all periods. All times are Pacific Daylight Time unless otherwise specified. MABL turbulent kinetic energy dissipation rate derived u*'s were obtained from velocity fluctuation measurements from the R/V Acania main mast (at 20 m) and a bow mast (at 5 m) instruments. MLD data were obtained from CTD casts from the R/V Acania for Case I and by the R/P FLIP for Cases II and III.

Conditions associated with these cases was dominated by increasing clouds, swell and winds with intermittent to heavy rainfall. Heavy rain showers occurred on 29 October when the first of several fronts passed through the area. Since the presence of fog, rain or drizzle affects the validity of the hot film signals used in the dissipation technique, care was taken to exclude affected results during the periods.

Ocean conditions were also variable. MILDEX experiment participants reported large scale advection and upwelling occurred during the course of the experiment. Significant internal wave activity was also evident and is being analyzed by other investigators.

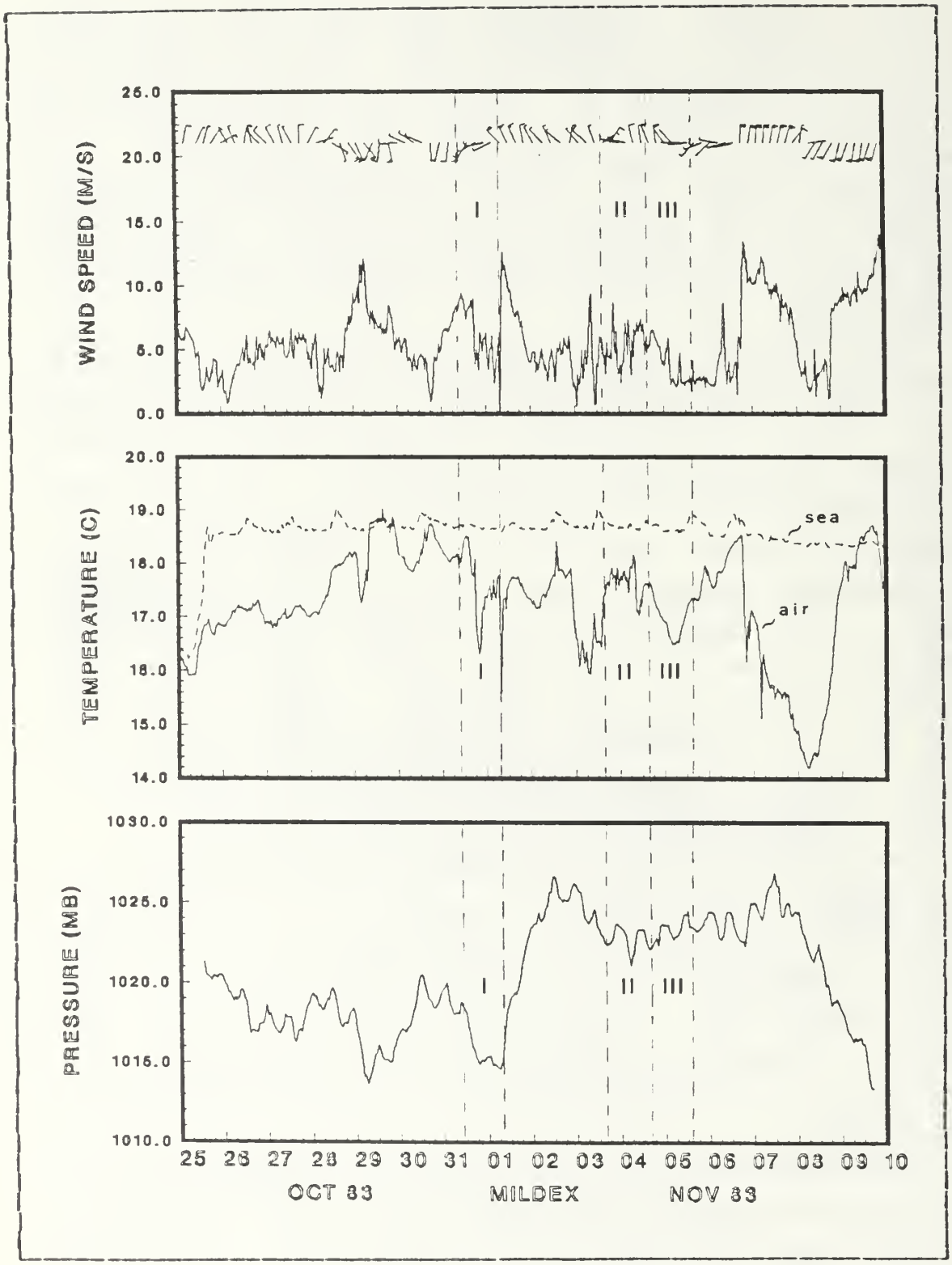

Fig. 3.2 Time Series of MILDEX Wind Speed and Direction, SST, Air Temperature, and Surface Pressure. Times are PDT.

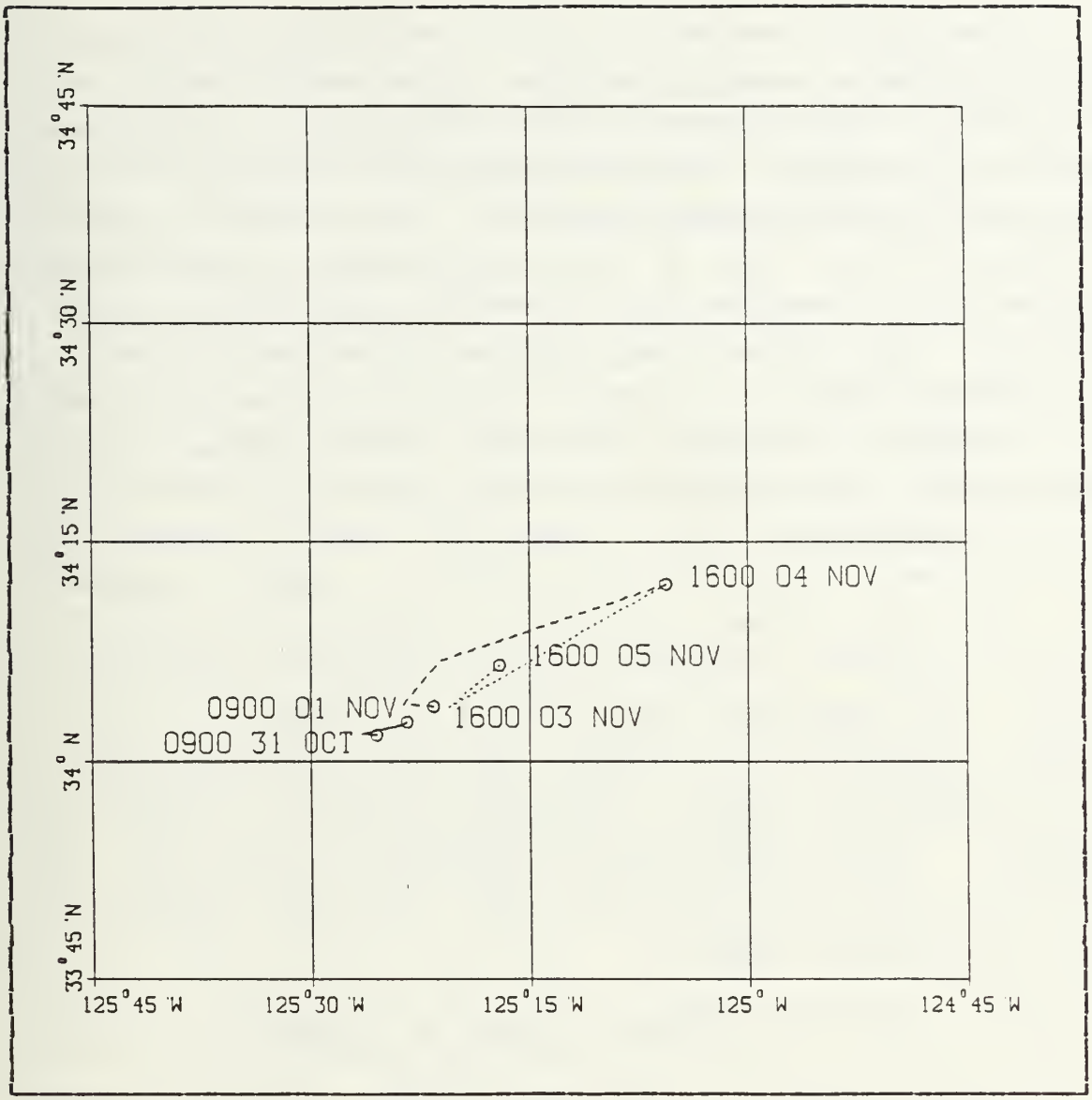

Fig. 3.3 Movement of R/V Acania: Case I (solid), Case II (dash), Case III (dot).

B. CASE I (0900, 31 OCTOBER - 0900, 01 NOVEMBER)

During this period, the R/V Acania experienced weak cold frontal passage at about 1700 on 31 October. Fig. 3.4 shows the National Meteorological Center (NMC) surface analysis for Case I. The synoptic situation was that a low center

was located in the northeast Pacific ocean, and a high dominated the Pacific north of Hawaii. The entire period had nearly 100% cloud cover and intermittent rain or drizzle. Several rain squalls were noted after the frontal passage. Clouds varied from altostratus prior to the frontal passage to stratus for the rest of the Case I period. No fog was reported, so a considerable amount of hot film data was available. Fig. 3.5 is a copy of GOES WEST visual imagery.

As shown in Fig. 3.2, winds were initially from the SSW with a shift to the west after the frontal passage with speeds varying from 7 to 9 m/s ahead of the front and from 3 to 5 m/s behind the front. There was a steady decrease in surface pressure from 1018 mb to 1014 mb. Swells increased from 4 to 9 ft after the frontal passage and gradually decreased to 5 ft towards the end of the observational period. Air temperature dropped by 1.5°C after the frontal passage. Throughout the period, the SST was greater than the air temperature with the greatest difference at night as expected. Air-sea temperature differences varied from -.2° to -2.3° C. The MABL surface layer was near neutral to unstable during the period.

C. CASE II (1600, 03 NOVEMBER - 1600, 04 NOVEMBER)

During this period, a stronger cold front than in Case I was approaching. Fig. 3.6 is the NMC surface analysis for Case II. A low center was positioned in the Gulf of Alaska, and a high pressure center had intensified west of Baja California and south of the Acania. No frontal passage was observed for this case. Winds were generally from the NNW shifting to the west in the middle of the observational period and then returned to the NNW at the end while wind speeds fluctuated between 3 and 7 m/s. The surface pressure was very steady changing only by 2 mb from 1021 to 1023 mb.

Swells were significant and from the NW and ranged from 7 to 9 ft. Fluctuations in air temperature never exceeded 1.0°C. As in Case I, the SST was greater than the air temperature with the air-sea temperature difference varying from -.6°to -1.6°C. In this case, the MAEL surface layer was unstable throughout the entire period.

Fig. 3.7 shows GOES WEST visual imagery for this case. Cloud cover was heavy in the late afternoon and again at mid-morning on the next day. During the night, the sky was cloud-free. Fog, cumulus and stratus clouds were evident in the afternoon. Stratus with some cirrus was present the next morning. No precipitation was recorded during the Case II period.

D. CASE III (1600, 04 NOVEMBER - 1600, 05 NOVEMBER)

The cold front approaching during Case II dissipated at the beginning of the period and the area came under the influence of a weak high pressure south of the R/V Acania. Fig. 3.8 is the NMC surface analysis for Case III. Another low pressure system is to the NW with an associated cold front. This second system did not appear to influence the weather or the seas in this case. Winds initially were from the NNW and gradually shifted to the SSW as the high moved through the area. Speeds generally decreased from about 7 to 2 m/s, and air temperature fluctuated no more than .7°C. Surface pressure varied by 2 mb from 1022 to 1024 mb while sea swells were from the NW at 8 to 10 ft. As in the previous two cases, the SST was greater than the air temperature with the air-sea temperature difference varying from -1.1°to -2.1°C. Again, the MABI was unstable for the entire period.

This last case had the least cloud cover due to the influence of the high pressure system. Fig. 3.9 shows GOES

WEST visual imagery for Case III. At the beginning of the period, 50% cloud cover, consisting mainly of stratocumulus, was evident. This changed to cirrus and finally a clear night-time sky. On the morning of 5 Nov. there was 30% to 50% cloud cover (mostly cirrus and some cumulus) with clearing in the afternoon. Nc precipitation was recorded for this period which was good for hot film performance.

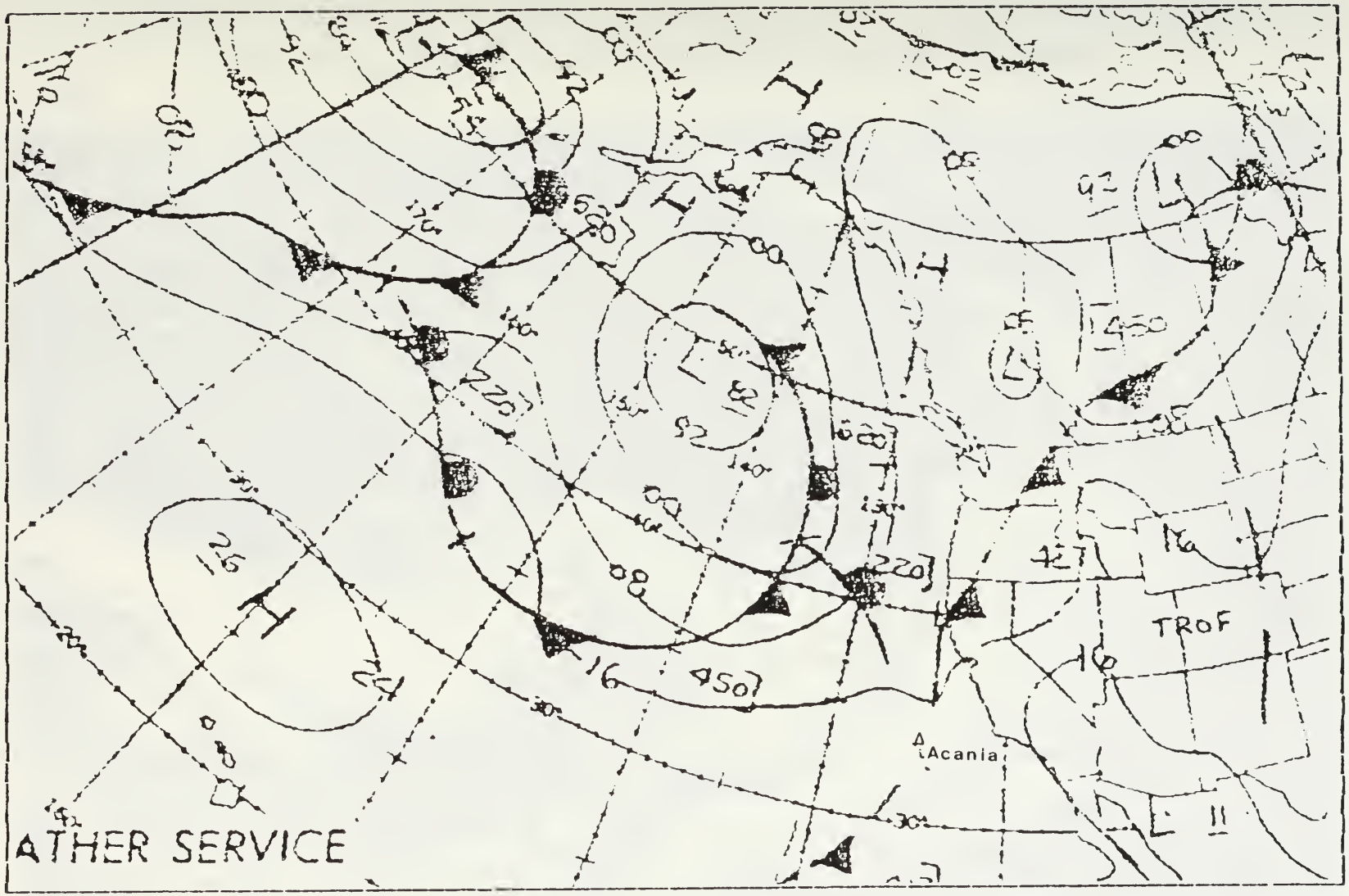

Fig. 3.4 NMC Surface Analysis 1200 GMT OCTOBER 31,1983

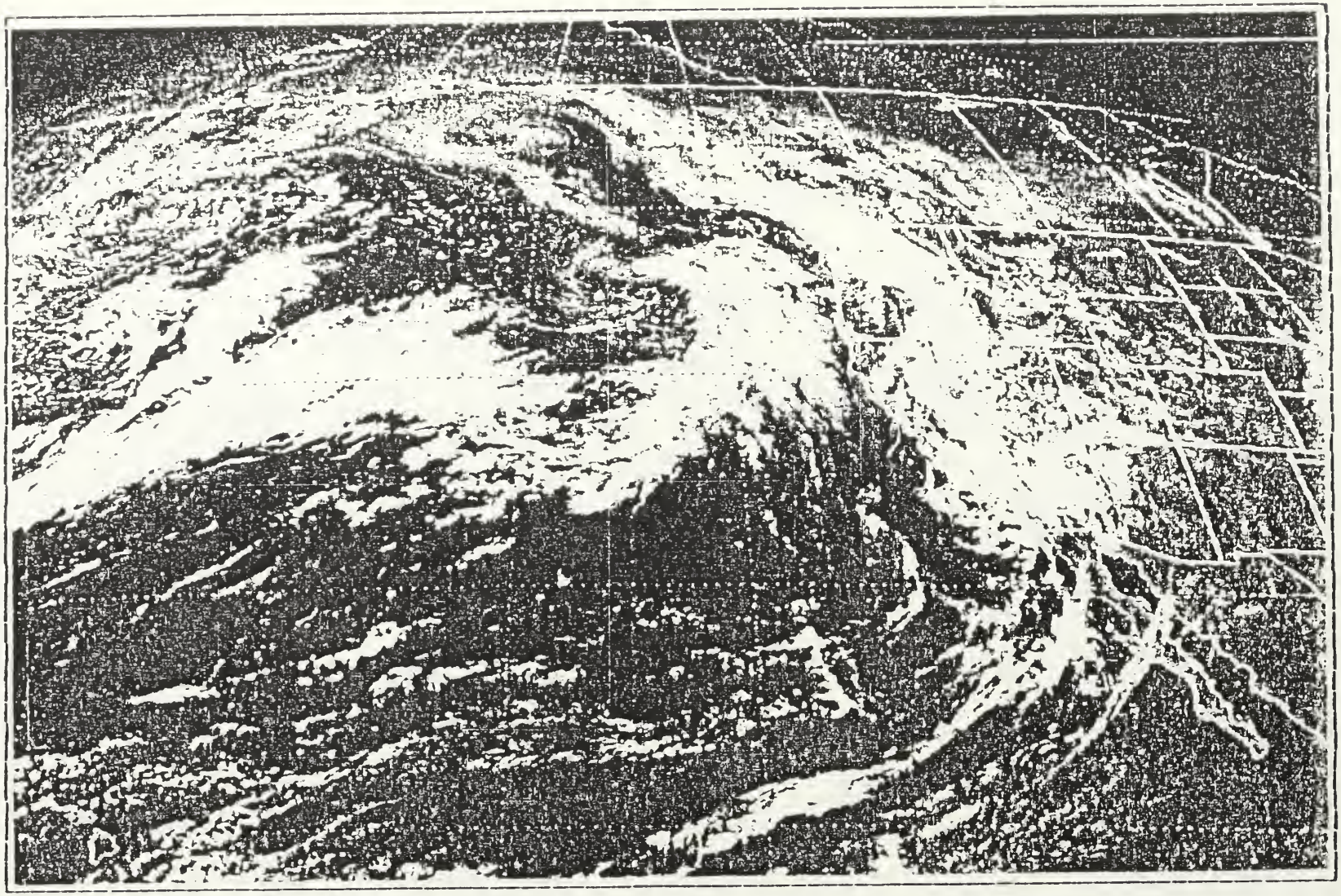

Fig. 3.5 GOES WEST Visual 2215 GMT NOVEMBER 01, 1983

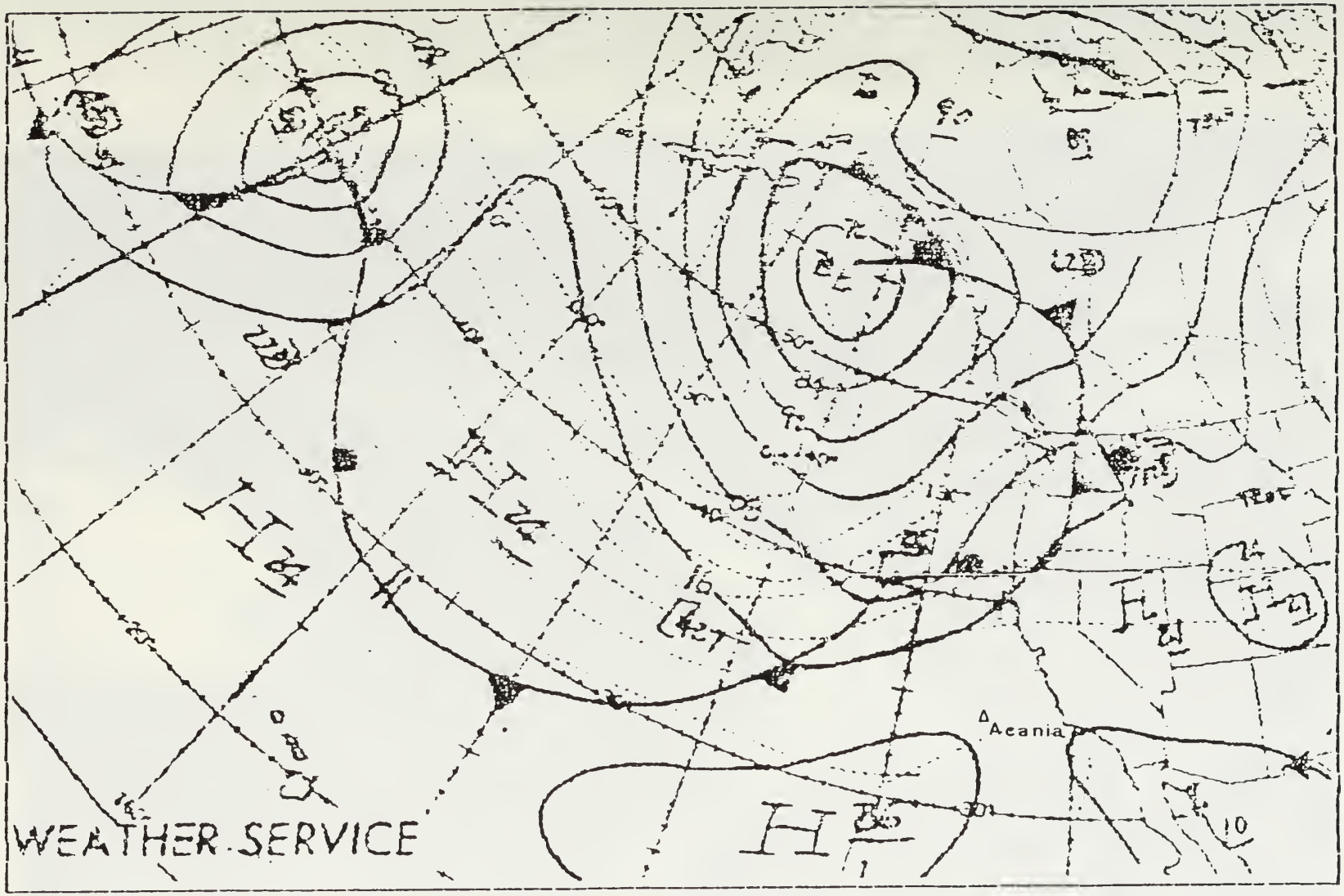

Fig. 3.6 NMC Surface Analysis 1200 GMT NOVEMBER 03, 1983

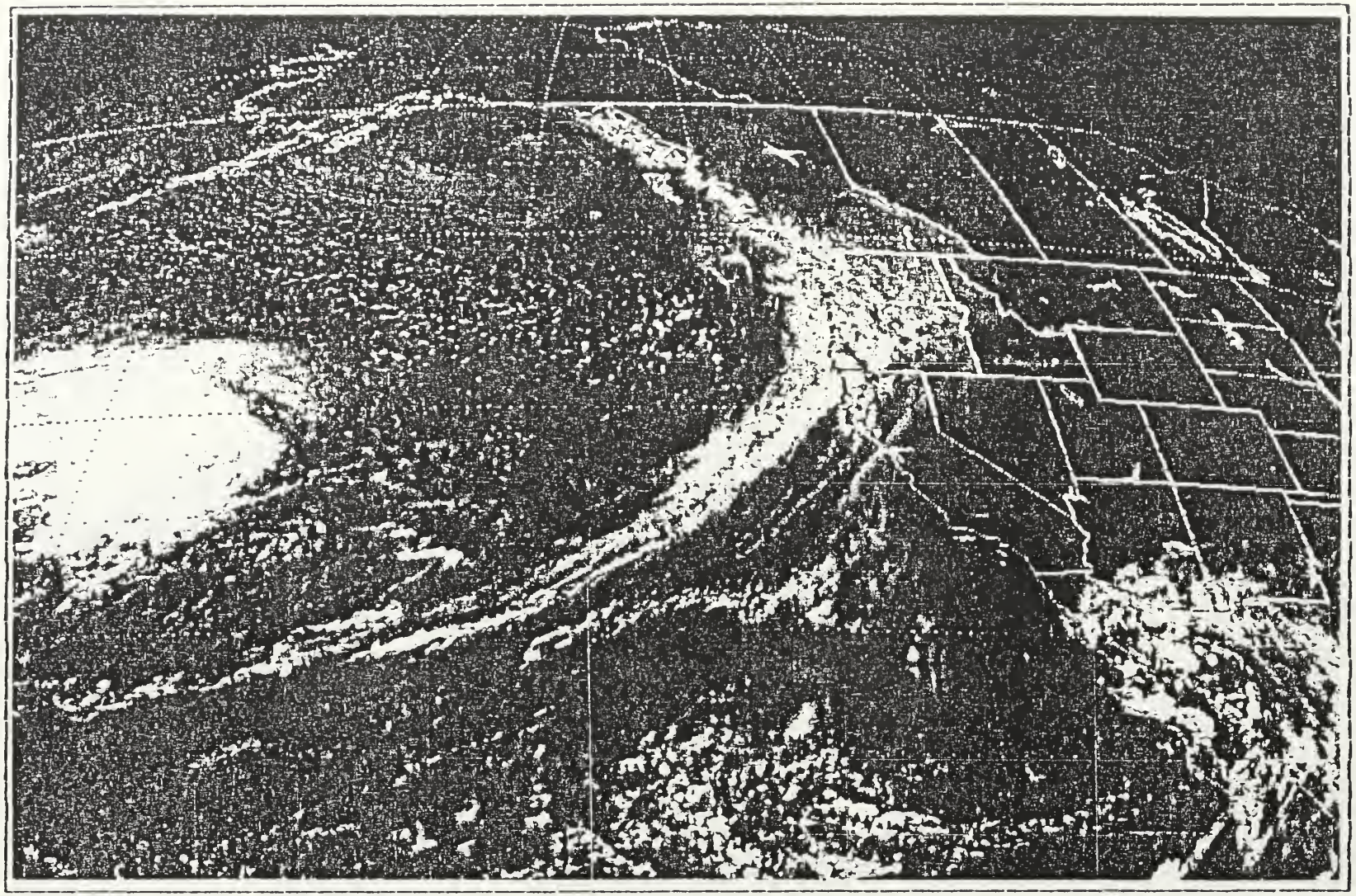

Fig. 3.7 GOES WEST Visual 2215 GMT NOVEMBER 03, 1983

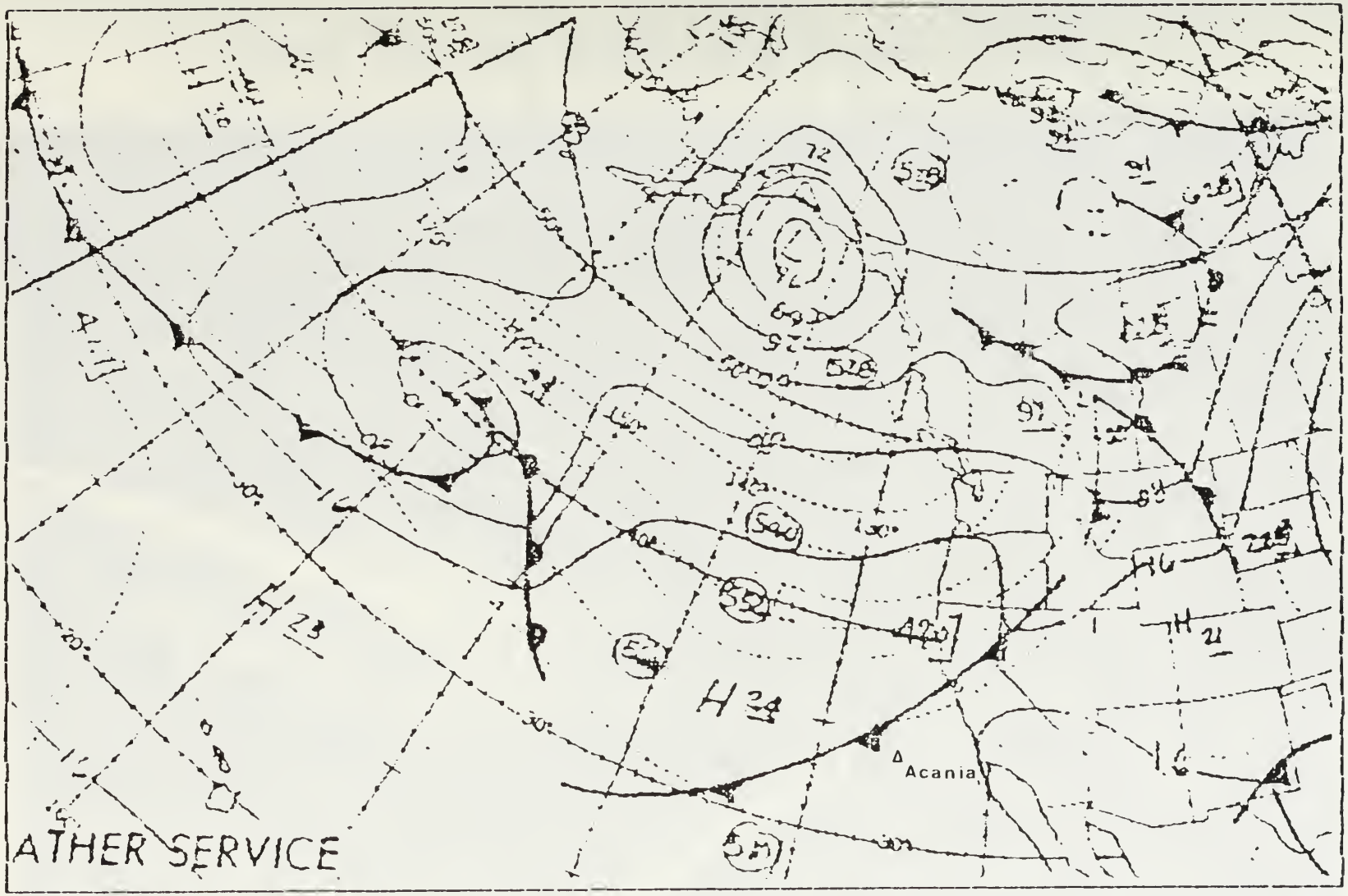

Fig. 3.8 NMC Surface Analysis 1200 GMT NOVEMBER 04, 1983

Fig. 3.9 GOES WEST Visual 2315 GMT NOVEMBER 04, 1983

IV. DATA AND RESULTS

A. APPROACH TO FORCING U* INTERPRETATION

For each of the three cases, the u* associated with the model predictions was compared with the TKE dissipation rate (ϵ) derived u* and the model MLD was compared with the observed MLD. As described previously, the epsilon (ϵ) estimates necessary for u* calculations by this method were obtained from hot film measurements on the bow (5 m) and main masts (20 m) of the R/V Acania (Fig. 3.1).

The MABL model is configured for ten input winds, so the ten greatest and least winds were chosen from each 24-hour period. These will be referred to in the discussion as "peak" winds. Linear interpolation was used for data points between these ten points. However, a forecaster at sea would not predict high and low winds, but would most likely forecast average winds over the period. Therefore, another model run utilizing 2.5 hour wind averaging was input over the same periods to see if the use of averaged winds would have any deleterious effect on the MLD computations.

The purpose of these comparisons is to evaluate atmospheric forcing (u*) in relation to predicted and observed MLD's. There are three u*'s used in this study: those estimated by bulk formulations using peak winds, by bulk formulations using averaged winds, and by dissipation estimates. In the following discussion, the first two sets will be referred to as model u* (peak or averaged) and the last set as dissipation u*.

B. CASE I (0900, 31 OCTOBER - 0900, 01 NOVEMBER)

This first case resulted in the poorest comparison of predicted and observed values of any of the three cases. Initialization data is summarized in Table I. Table II lists the 2.5 hour averaged winds that were used for subsequent runs. In Fig. 4.1, a comparison of the two wind inputs is shown. Fig. 4.2 shows a comparison of u*'s. A difficulty in comparing model and instrument derived values for this case was instrument performance and equipment breakdown. Both of these problems were encountered.

TABLE I

Case One Initialization

Atmospheric Values

Pressure: 1019.0 mb — Sea Temp (C): 18.64
Pot. T(C): 17.9 — Spec. Hum: 10.47
Lift. Cond. Lvl: 351.74m — Advection: 0.

Ocean Values

Mixed Layer Depth: 34.5m — Temp. Jump (C): -.16
Below Layer Gradient: -.0155

Winds

Time(PDT)	Speed(m/s)	Direction
0900	8.3	181.0
1120	9.5	176.0
1345	7.4	205.0
1745	9.1	199.0
2030	3.4	218.0
2130	6.4	215.0
0140	3.5	259.0
0345	6.1	247.0
0505	2.4	230.0
0720	5.9	294.0

Rain, drizzle, and low relative wind speeds affected the accuracy of both the bow and main mast dissipation derived

TABLE II

Case One Averaged Winds

Time (PDT)	Speed (m/s)	Direction
0900	8.3	181.0
1130	8.9	178.0
1400	8.2	203.0
1630	8.6	196.0
1900	4.6	263.0
2130	5.4	221.0
0000	5.7	253.0
0230	4.5	253.0
0500	4.2	231.0
0730	4.9	295.0

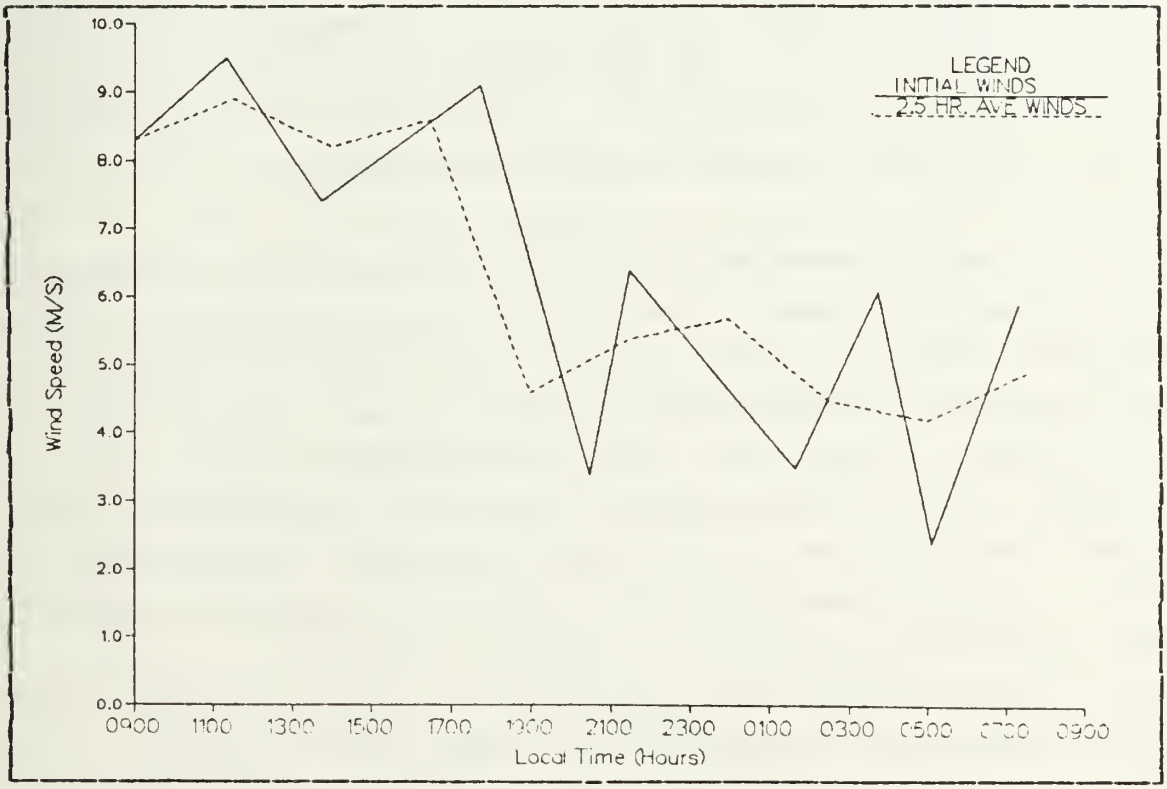

Fig. 4.1 Comparison of Case I Initial and Averaged Winds.

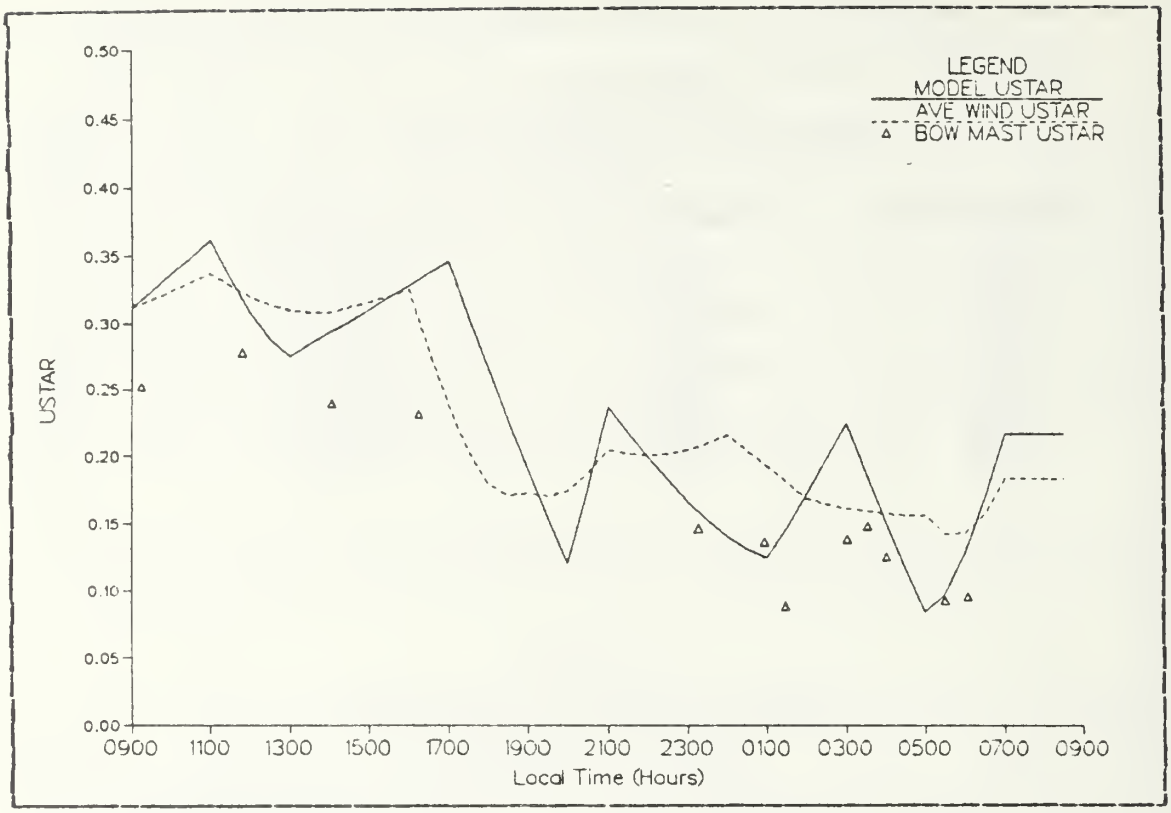

Fig. 4.2 Case I Friction Velocities

u* values. Post-processing removal of the bad data resulted in significant data gaps. For the bow mast, dissipation u* values are missing from 1616 to 2315 and from 0604 onward. Only 12 useable observed data points were available (as compared to 48 for the model) for the period. The field log indicates a lack of confidence in main mast spectra by the observers onboard due to spurious voltage readings and connector problems, so data from it were not included at all in this comparison.

Fig. 4.2 shows the peak wind and averaged wind model u* and the dissipation u* values. As expected, the model u* values are a function of the differences in the input winds. Where the averaged winds are higher, the u*'s are higher. The dissipation u* values obtained from the bow mast have

the same trend but are lower than both model u*'s in the pre-frontal period (before 1700). They are close to the "peaked" wind model predictions for the rest of the time. All of the u* dissipation values are lower than the averaged wind model predictions.

These results of model and dissipation u* values were not completely expected for the frontal regime. Previous comparisons of bulk and dissipation u*'s in frontal regions (Geernaert, et al., 1985) indicated that the dissipation u*'s were higher than bulk values prior to a frontal passage and then the magnitudes reversed after the passage. Here the dissipation u*'s remained lower than the bulk value throughout. Generally, the study is revealing that small pre-frontal wind speeds (less than 6 m/s) produce greater u* deviations (turbulent vs bulk). Additionally, if the swell and wind oppose each other, greater u* deviations were also evident. These were minimized if the wind and swell were at right angles to each other. The reasons for this are not entirely clear. However, it has been postulated (Geenaert, et al., 1985) that the direction and magnitude of the swell relative to the wind (primarily the interaction of wind stress with short wave elements on long wave crests) affects the roughness length, z_o, which in turn affects u* and C_d.

No attempt will be made with these results to examine how the swell interacted with the wind and how this could have modified the u* values. Perhaps this case did not have the same kind of swell-wind interaction as in previous studies. This is an area for further investigation.

Fig. 4.3 compares the model and observed MLD's. The model prediction was based on bulk u* values shown in Fig. 4.2. In this case, model results (solid line) early in the period do not agree with the observed MLD (dashed line). While both curves nearly coincide at the start, the model curve shallows much more quickly although it reaches the

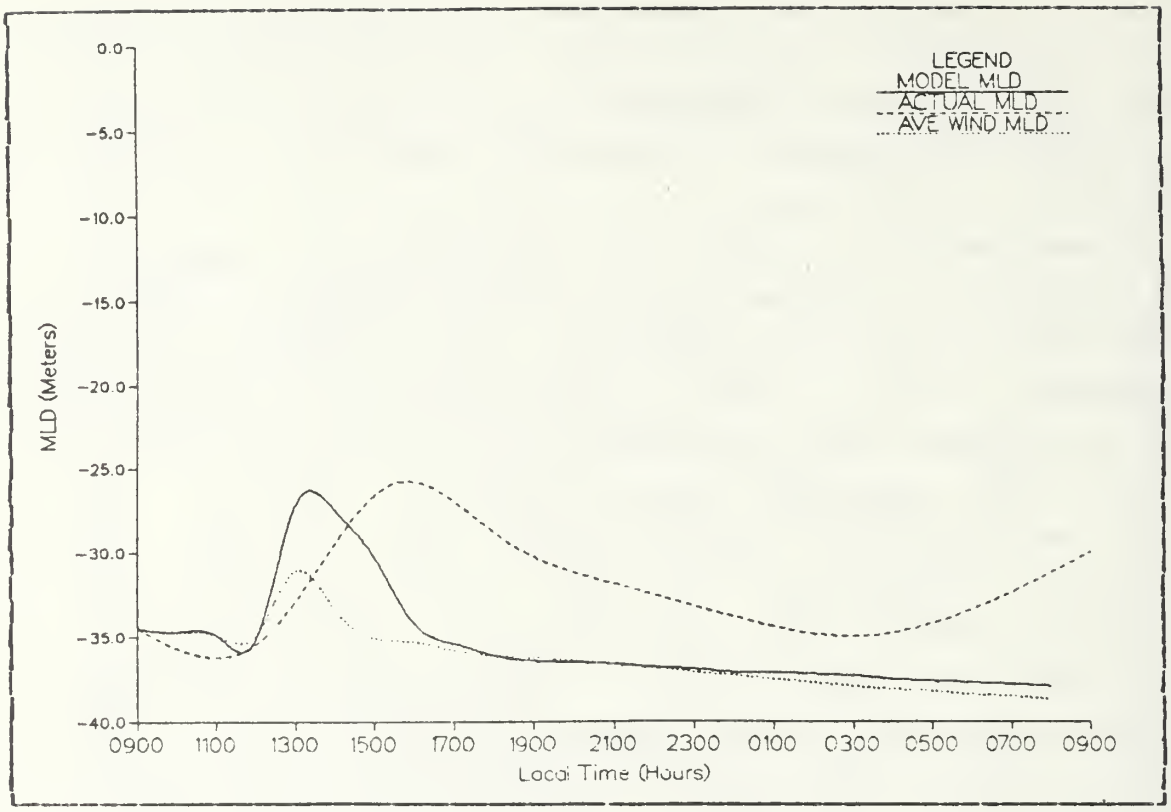

Fig. 4.3 Case I Mixed Layer Depth

proper depth. Then the model deepens rapidly and stays significantly deeper for the rest of the case. An MLD error of up to 10 meters can be tactically significant for naval forces in predicting sonar perfcrmance.

The early shallowing may not constitute a model prediction error. A CTD cast would give the thermal MLD while the model predicts the turbulent boundary layer depth. It takes a finite amount of time for the temperature field to adjust to the turbulent field. The expression for the lag is:

$$t \sim [(\Delta T)\, u^{*3}]/Q_o^{\,2} \qquad (4.1)$$

where:

T = temperature

t = lag time

Q_o = surface heating

Thus based on equation 4.1, the greater the u*, the greater the lag and the greater the heating (Q_o), the less the lag.

Using 2.5 hour averaged winds showed no improvement in MLD prediction (Fig. 4.3 dotted line) and in fact gave a poorer prediction. While the two wind inputs (Fig. 4.1) are quite different, the output MLD's are quite close together except at 1300. This is a pre-frontal period of strong winds and, from 1200 to 1700, the averaged wind speeds are higher than the initial winds. Since MLD is a function of the wind speed cubed, the stronger winds would give deeper mixing. This is again true for the period from 2300 to the end of the run where the averaged winds are generally higher than the initial winds. Overall, one can conclude that for this case both the "peaked" and averaged winds give poor MLD predictions and these could have adverse effects for naval operations. However, if the dissipation u* values for 0900 to 1700 (which are lower than the bulk values) had been used by the model, the model MLD would have been closer to the observed.

C. CASE II (1600, 03 NOVEMBER - 1600, 04 NOVEMBER)

The coupled model MLD prediction agreed well with the observed MLD changes in this case. The model predicted unstable ABL conditions throughout the period which agreed well with observations. Table III contains the initialization data for this case and the 2.5 hour averaged winds are listed in Table IV. Fig. 4.4 compares the two input winds for this case.

This was a period with unreliable dissipation u* data. Fig. 4.5 is a plot of the various friction velocities.

TABLE III

Case Two Initialization

Atmospheric Values

Pressure: 1022.4 mb
Pot. T(C): 17.1
Lift. Cond. Lvl: 476.71m
Sea Temp (C): 18.78
Spec. Hum: 9.32
Advection: 0.

Ocean Values

Mixed Layer Depth: 12.0m
Below Layer Gradient: -.0094
Temp. Jump (C): -.2

Winds

Time(PDT)	Speed(m/s)	Direction
1600	4.0	040.0
1745	5.6	310.0
2120	8.6	036.0
2230	4.7	319.0
2300	6.4	355.0
0135	2.4	270.0
0400	7.0	281.0
0705	3.0	350.0
1005	7.2	008.0
1420	4.6	336.0

While fog or rain were not a factor in dissipation measurements, equipment failure was a problem. This led to a reduction of dissipation u* data. The bow mast data were not available from 1700 to 2300, 2330 to 0217, and 0900 to 1600 when a major equipment repair was accomplished. Bow dissipation u* data from 12 thirty minute periods were available. Main mast dissipation measurements were not available from 1600 tc 0752 and from 0822 to 1340. It was also absent after 1410 and only data from 4 thirty minute periods were available.

At the beginning of the period, the bow mast dissipation u*'s are close to the bulk derived (model) values. However, during the middle part of the period, the bow dissipation values are consistently lower than the bulk (model) although

TABLE IV

Case Two Averaged Winds

Time (PDT)	Speed (m/s)	Direction
1600	3.9	040.0
1830	4.5	345.0
2100	5.7	349.0
2330	4.3	308.0
0200	3.6	274.0
0430	6.1	282.0
0700	4.6	307.0
0930	6.6	357.0
1200	6.8	348.0
1430	5.4	341.0

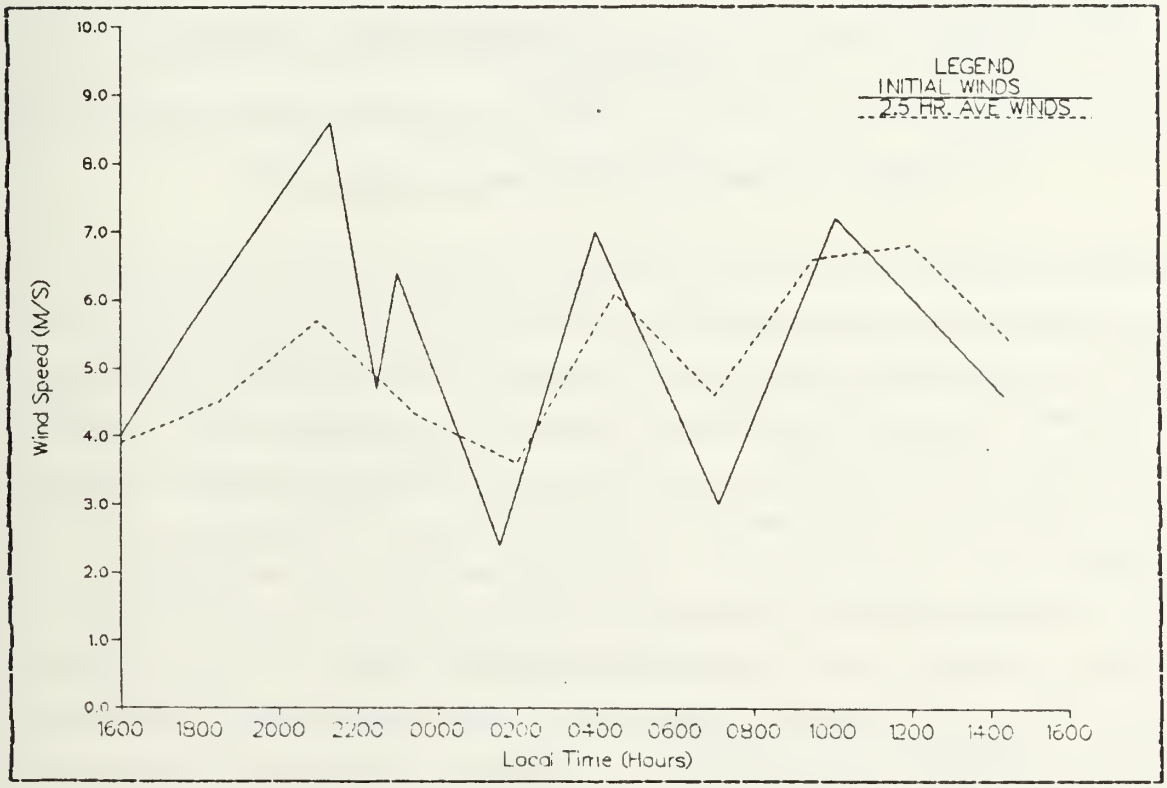

Fig. 4.4 Comparison of Case II Initial and Averaged Winds.

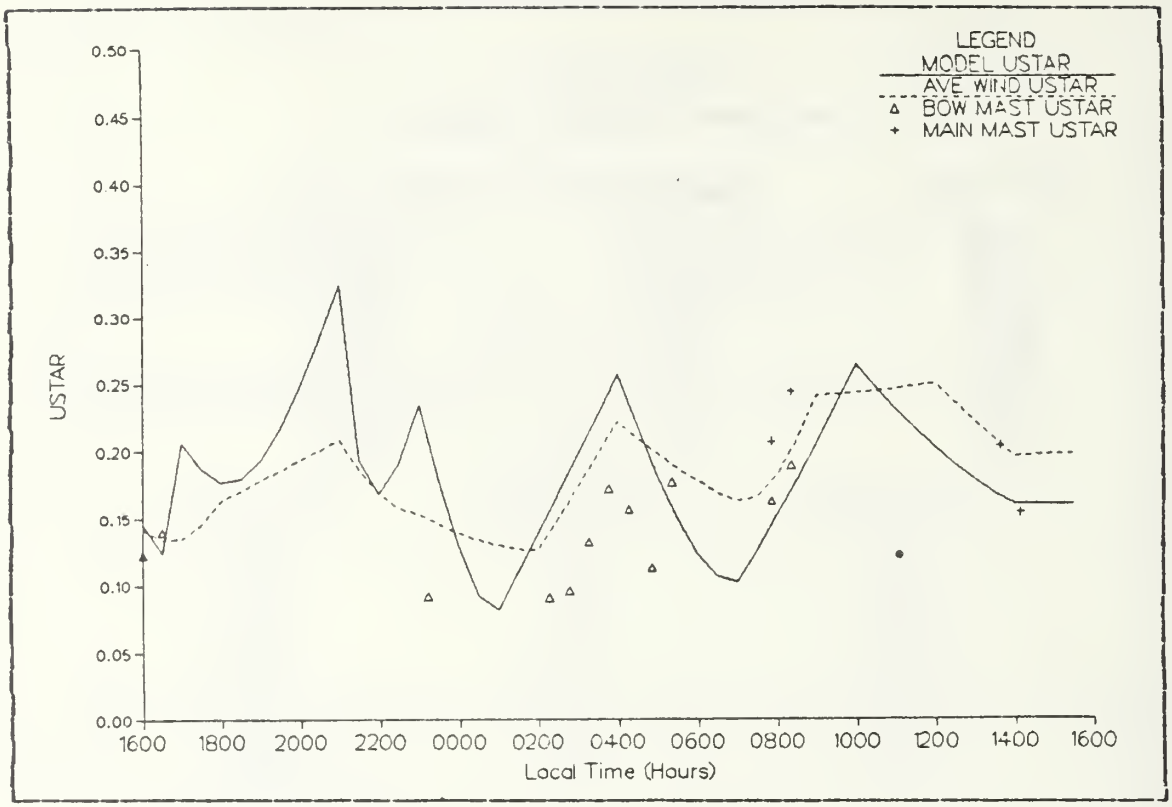

Fig. 4.5 Case II Friction Velocity

they tend to have the same time variations. The two bow u* dissipation values near 0800 are close to the model values.

It is apparent from Fig. 4.6 that the model predicted the MLD well enough for Naval tactical applications. The observed MLD (dashed line) shows some differences from 0200 to 1000 which are probably due to internal wave activity, advection or as a result of the ship moving to a different area. Observed MLD data was not available for 1100 to 1300. This contributes to the abrupt MLD rise at 1400. The model (solid line) predicted the MLD quite well especially for the deepening part of the period. Better agreement between observed and model shallowing would probably be evident if MLD data would have been available for 1100 to 1300.

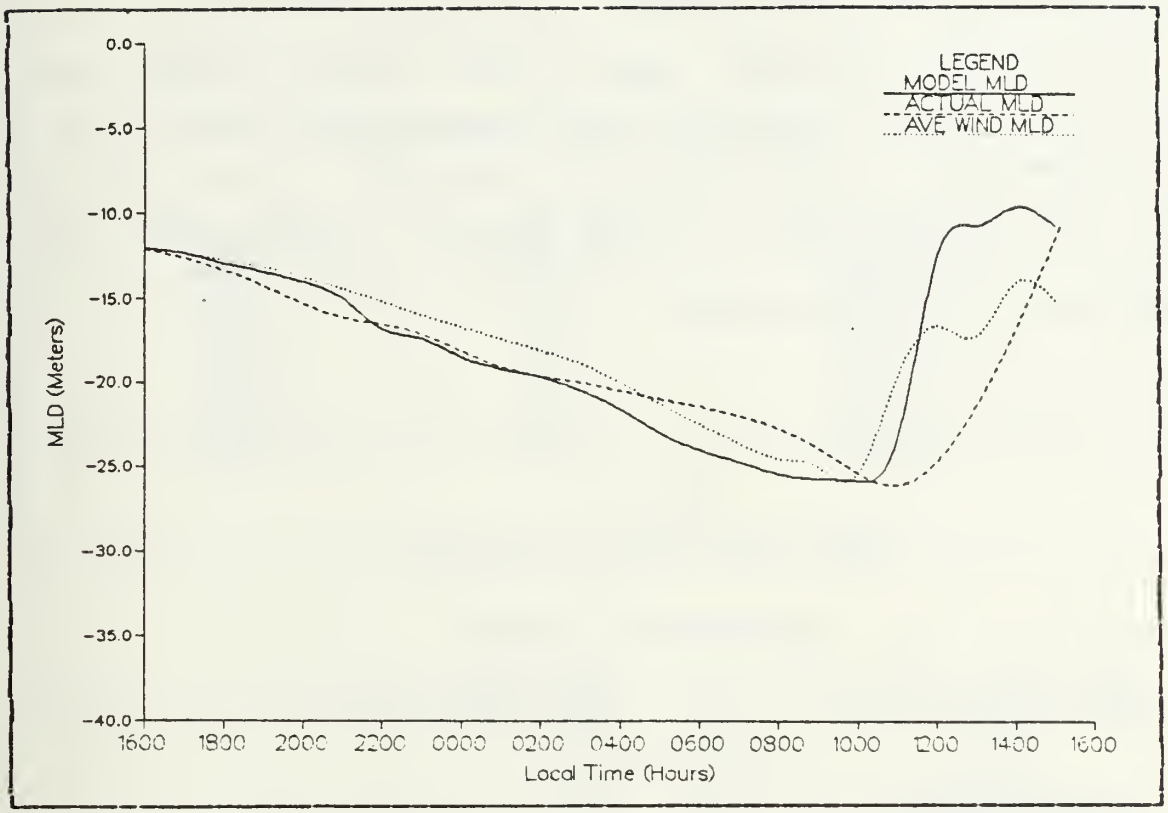

Fig. 4.6 Case II Mixed Layer Depth

Comparison of the peaked winds with the 2.5 hour averaged wind MLD's yields some interesting results. During the deepening phase, the averaged winds consistently give a shallower MLD (dotted line) than the initial winds. At this time the "peaked" winds are consistently stronger (Fig. 4.4) than the averaged winds (except at 0100) and would produce more vigorous mixing. However, during the shallowing portion, the averaged wind prediction is significantly deeper than the peaked wind prediction. This time the averaged winds are predominantly stronger than the peaked winds. Again the predicted MLD results are expected since the MLD is proportional to u^{*3}. If the dissipation u* values for 0200 - 0600 would have been used by the model, the predicted MLD would have been shallower for that period and closer to the observed.

D. CASE III (1600, 04 NOVEMBER - 1600, 05 NOVEMBER)

As in the previous case, the coupled model MLD predictions agreed well with the observed conditions. ABL conditions were unstable throughout the case. Table V lists the initialization data utilized for this model run, and Table VI lists the 2.5 hour averaged winds. Fig. 4.7 compares the two input winds.

TABLE V

Case Three Initialization

Atmospheric Values

Pressure: 1022.3 mb
Pot. T(C): 17.7
Lift. Cond. Lvl: 508.0m
Sea Temp (C): 18.70
Spec. Hum: 9.48
Advection: 0.

Ocean Values

Mixed Layer Depth: 11.5m
Below Layer Gradient: -.0053
Temp. Jump (C): -.1

Winds

Time(PDT)	Speed(m/s)	Direction
1600	5.2	340.0
1755	6.5	338.0
2100	5.6	351.0
2300	4.5	352.0
0046	3.7	338.0
0155	5.2	325.0
0445	2.6	020.0
0715	2.1	296.0
0915	4.8	333.0
1045	2.4	271.0

This case had no fog related problems affecting the dissipation data but for some periods, the low relative wind speeds degraded dissipation reliability. Several large dissipation data gaps resulted. For the bow mast, data gaps exist for 1600 to 0018, 0100 to 0815, 0845 to 1200, and from

TABLE VI

Case Three Averaged Winds

Time (PDT)	Speed (m/s)	Direction
1600	5.4	340.0
1830	6.0	340.0
2100	5.6	351.0
2330	4.3	346.0
0200	5.0	354.0
0430	2.7	004.0
0700	2.3	311.0
0930	3.2	272.0
1200	2.5	264.0
1430	2.3	235.0

Fig. 4.7 Comparison of Case III Initial and Averaged Winds.

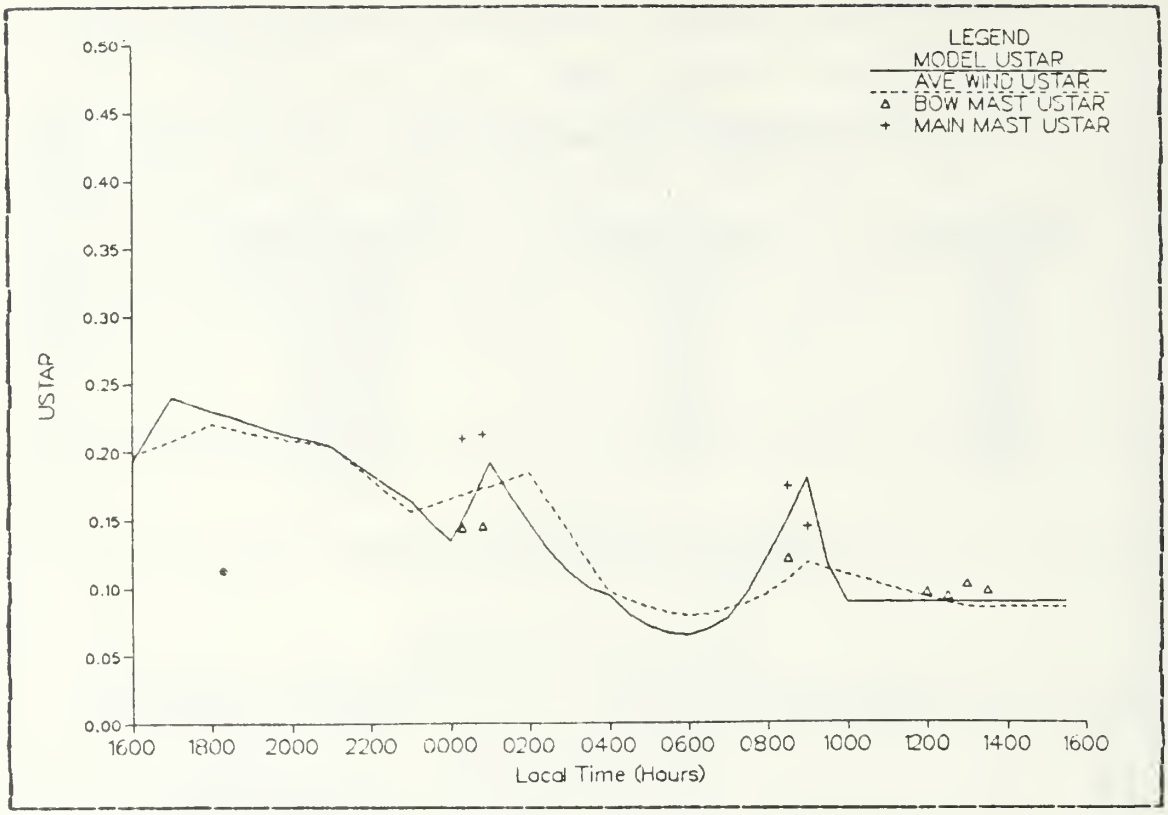

Fig. 4.8 Case III Friction Velocities

1331 onward. Only seven reliable dissipation values were calculated for the bow mast. Data was not available for the main mast from 1600 to 0018, 0100 to 0815, and from 1410 to the end of the period. This resulted in four thirty-minute dissipation averages. Fig. 4.8 compares the different friction velocities.

For the entire period, the peak and averaged wind model u*'s are very close due to the small wind differences between the two (Fig. 4.7). Both the main mast and bow mast dissipation u*'s agree reasonably with u*'s from the peaked wind model run. This is particularly true in the second half of the period. Some variation is expected since the dissipation u* comes from instantaneous measurements, while the model uses interpolated values between the input winds.

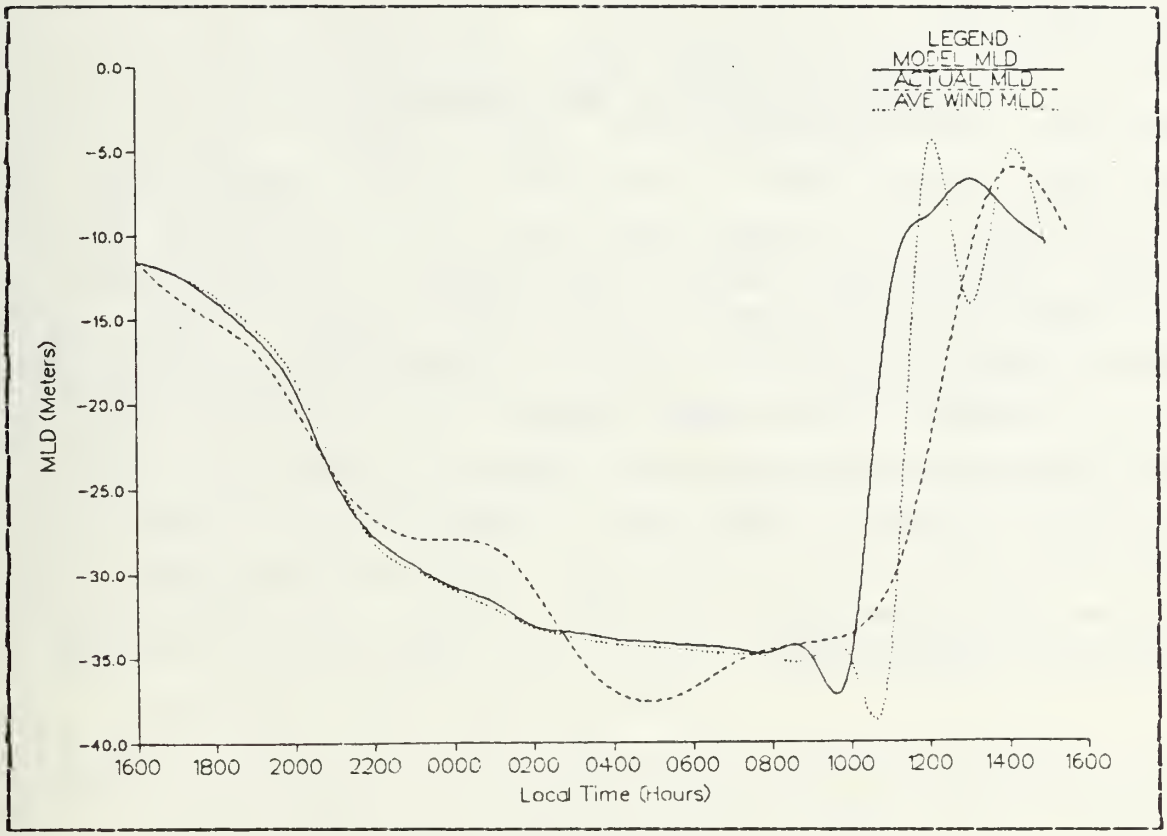

Fig. 4.9 Case III Mixed Layer Depth

The model also predicted the MLD's well (Fig. 4.9) although there is greater deviation from the observed (dashed line) than in Case II. As before, the actual MLD shows some internal wave or advective features (particularly around 0000 and 0400). Good observed MLD data was available for the entire period.

The initial model run (solid line) agrees well in the initial stages but deviates during the above mentioned internal wave or advective events. The sharp "dip" at about 0930, not present in the model output, is an artifact introduced by use of a spline interpolation in the plotting routine. The model also shallows to the proper depth but it occurs about one hour early.

Comparing the averaged winds MLD with the peak winds MLD shows that both are very similar. The plot of input winds (Fig. 4.7) shows that both the initial and averaged winds were very close throughout the period except between 0800 and 1000, so both model runs should produce similar MLD's. After 1100, the averaged wind MLD (Fig. 4.9 dotted line) shows a double maxima during shallowing. It is unknown at this time why the model predicted such maxima. They have been slightly exaggerated by use of the spline interpolation but are present in the model output. As with the initial wind MLD, an anomolous "dip" is observed at 1030 also due to the spline interpolation. Both the initial and averaged wind MLD's are within operational tolerances for Navy use but the forecaster should be well versed in the model properties and limitations.

V. CONCLUSIONS AND RECOMMENDATIONS

A. CONCLUSIONS

The coupled model has been subject to various past analyses and performed well. This study has examined the performance of the model in regimes that stretch its capabilities. Several important conclusions can be drawn:

(1) The model overpredicts clouds which affects short and long wave radiative effects on boundary layer dynamics.

(2) Good comparisons of bulk and dissipation u* for unstable conditions are made.

(3) In near neutral or slightly unstable regimes, u* predictions vary systematically probably due to swell and wind stress interaction.

(4) Better predictions are achieved if peak winds instead of averaged winds are used. However, a forecaster would only have average wind prediction estimates available at the time of operationally initializing the model.

(5) Given reasonable fluxes of short and long wave radiation, the model predicts routinely observed variations in ocean mixed layer depth.

(6) It is a potentially powerful tool and an aid in single-station forecasting to a Naval Oceanographer who is aware of the model limitations.

The model performed very well within its limitations. However, further work needs to be done before it can be implemented in an operational role.

B. RECOMMENDATIONS

In order to facilitate operational usage, several areas should be explored. Some of the aforementioned problems could be alleviated by attempting the following recommendations:

(1) Continue research and development of the coupled model with direction toward operational implementation.

(2) When clouds form, the model assumes them to extent from horizon to horizon. This is unrealistic and a statistical probability of percentage cloud cover should be added. Partial cloud cover would also alter short and long wave effects on boundary layer dynamics.

(3) Incorporate swell and wind interaction effects into u* calculations based on bulk formulae.

(4) Continue to analyze MILDEX data, particularly for periods where there are more complete dissipation u*'s.

(5) Plan for model coupling to other predictive models such as IREPS and ICAPS.

(6) Involve students in at-sea data gathering experiments. This would enhance understanding of thesis research and minimize "false starts" due to attempting cases with faulty or limited data.

The model has tremendous potential. Performing further analysis and tweaking the model will result in a powerful tool for the fleet; one that can be used in times of crisis when extensive satellite networks may not be available for use by forecasters.

LIST OF REFERENCES

Champagne, F.H., C.A. Friehe, J.C. LaRue, and J.C. Wyngaard, 1977: Flux measurements, flux estimation techniques, and fine structure turbulence measurements in the unstable surface layer over land. J. Atmos. Sci., 34 513-530.

Davidson, K.L., C.W. Fairall, P.J. Boyle, and G.E. Schacher, 1984: Verification of an atmospheric mixed-layer model for a coastal region. J. Clim. Appl. Meteorol. (accepted), 28 pp.

Davidson, K.L. and R.W. Garwood, 1984: Coupled oceanic and atmospheric mixed layer model. Dynamics of Atmospheres and Oceans, 8, 283-296.

Fairall, C.W., K.L. Davidson, and G.E. Schacher, 1981: A review and evaluation of integrated atmospheric boundary-layer models for maritime applications. NPS-63-81-004, Naval Postgraduate School, Monterey, Ca., 89 pp.

Fleagle, R.G. and J.A. Businger, 1980: An Introduction to Atmospheric Physics, 2nd ed., Academic Press, New York, New York, 432 pp.

Gallacher, P.C., A.A. Bird, R.W. Garwood Jr., and R.L. Elsberry, 1983: A determination of the constants for a second order closure turbulence model from geophysical data. Naval Postgraduate Technical Report, NPS-63-83-004, 35 pp.

Garwood, R.W., Jr., 1977: An ocean mixed layer model capable of simulating cyclic states. J. Phys. Oceanogr., 7, 455-468.

Geernaert, G.L., K.L. Davidson, P.J. Boyle, 1985: Variation of the drag coefficient and wind-wave coupling in the vicinity of a storm front. (unpublished report), 43 pp.

Geernaert, G.L., P.S. Guest, C.E. Skupniewicz, D.E. Spiel, K.L Davidson, W.J. Shaw, K.B. Katsaros, and R.J. Lind, 1983: Meteorology data report for the 1983 mixed layer dynamics experiment (MILDEX). NPS-63-84-002, Naval Postgraduate School, Monterey, Ca., 128 pp.

Gleason, J.P., 1982: Single-station Assessments of the synoptic-scale forcing on the marine atmospheric boundary layer. M.S. Thesis, Naval Postgraduate School, Monterey, Ca., 55 pp.

Husby, D.M. and G.R. Seckel, 1978: Large scale air-sea interactions at ocean station V. NOAA Tech. Rep. NMFS SSRF-696, 44 pp.

Joseph, J.H., W.J. Wiscombe, and J.A. Weinman, 1976: The delta-Eddington approximation for radiative flux transfer. J. Atmos. Sci., 31, 2452-2459.

Khalsa, S.J.S., and J.A. Bussinger, 1977: The drag coefficient as determined by the dissipation method and its relation to intermittent convection in the surface layer. Boundary-Layer Met., 12, 273-297.

Laevastu, T., 1960: Factors affecting the temperature of the surface layer of the ocean. Soc. Scient. Fenica. Comment. Physico.-Mathem., 25(1), 1-136.

Large, W.G., 1979: The turbulent fluxes of momentum and sensible heat over the ocean during moderate to strong winds. Ph.D. Dissertation, University of British Columbia, 180 pp.

Miller, J.R., 1976: The salinity effects in a mixed layer ocean model. J. Phys. Oceanogr., 6, 29-35.

O'Loughlin, M.C., 1982: Formulation of a prototype coupled atmospheric boundary-layer model. M.S. Thesis, Naval Postgraduate School, Monterey, Ca., 89 pp.

Oliver, V.J. and M.B. Oliver, 1945: Weather analysis from single station data. Handbook of Meteorology, F.A. Berry, E. Bollay, N.R. Beers, McGraw-Hill, New York, 858-879.

Schacher, G.E., K.L. Davidson, T. Houlihan, and C.W. Fairall, 1981: Measurements of the rate of dissipation of turbulent kinetic energy over the ocean. Boundary-Layer Met., 20, 321-330.

Seckel, G.R. and F.H. Beaudry, 1973: The radiation from sun and sky over the north pacific ocean. EOS, Trans. Am. Geophys. Union, 54, 1114.

Slingo, A.S., R. Brown, and C.L. Wrench, 1982: A field study of nocturnal stratocumulus: III. High resolution radiative and microphysical observations. Quart. J. Roy. Meteor. Soc., 108, 407-426.

Smithsonian Meteorological Tables. 1958: Fifth ed., Smithsonian Institution. 527 pp.

Staje, S.A. and J.A. Businger, 1981: A model for entrainment into a cloud-topped marine boundary layer-Part I: Model description and application to a cold air outbreak episode. J. Atmos. Sci., 38, 2213-2229.

Stage, S.A. and J.A. Businger, 1981: A model for entrainment into a cloud-topped marine boundary layer-Part II: Discussion of model behavior and comparison with other models. J. Atmos. Sci., 38, 2230-2242.

Tabata, S., 1964: A study of the main physical factors governing the oceanographic conditions of station P in the northwest pacific ocean. Ph.D. Thesis, University of Tokyo, 264 pp.

Tennekes, H. and A.G.M. Dreidonks, 1981: Basic entrainment equations for the atmospheric boundary layer. Boundary-Layer Met., 20, 515-531.

Wyngaard, J.C., and O.R. Cote, 1971: The budgets of turbulent kinetic energy and temperature variance in the atmospheric surface layer. J. Atmos. Sci., 28, 190-201.

BIBLIOGRAPHY

Byrne, Hugh M. "The Variation of the Drag Coefficient in the Marine Surface Layer Due to Temporal and Spatial Variations of the Surface Wind and Sea State", Ph.D. Thesis, University of Washington, 1982.

Davidson, K.L., G.E. Schacher, C.W. Fairall, P.J. Boyle and D.A. Brower. "Marine Atmospheric Boundary Layer Modelling for Tactical Use", NPS-63-82-001, Naval Postgraduate School, Monterey, Ca., September, 1982.

Dillon, Thomas M. and Thomas M. Powell. "Observations of a Surface Mixed Layer", Deep Sea Research, Vol 26A (1979), 915-932.

Garwood, R.W. Jr. "Air-Sea Interaction and Dynamics of the Surface Mixed Layer", Reviews of Geophysics and Space Physics, Vol 17, No 7 (October, 1979), 1507-1524.

Garwood, R.W. Jr., P. Muller and P.C. Gallacher. "Wind Direction and Equilibrium Mixed Layer Depth: General Theory", Unpublished Manuscript, 1984.

Garwood, R.W. Jr., P. Muller and P.C. Gallacher. "Wind Direction and Equilibrium Mixed Layer Depth in the Tropical Pacific Ocean", Unpublished Manuscript, 1984.

Geernaert, Gerald L., "Variation of the Drag Coefficient and Its Dependence on Sea State", Ph.D. Thesis, University of Washington, 1983.

James, Richard W. Ocean Thermal Structure Forecasting. Washington, D.C.: U.S. Naval Oceanographic Office, 1966.

Swaykos, J.W., "Simulation of the Coupled Atmospheric and Oceanic Boundary Layer Model During MILDEX", M.S. Thesis, Naval Postgraduate School, 1984.

INITIAL DISTRIBUTION LIST

		No. Copies
1.	Defense Technical Information Center Cameron Station Alexandria, VA 22314	2
2.	Library, Code 0142 Naval Postgraduate School Monterey, CA 93943	2
3.	Professor R.J. Renard, Code 63Rd Naval Postgraduate School Monterey, CA 93943	1
4.	Professor C.N.K. Mooers, Code 68Mr Naval Postgraduate School Monterey, CA 93943	1
5.	Professor K.L. Davidson, Code 63Ds Naval Postgraduate School Monterey, CA 93943	8
6.	Professor R.W. Garwood, Code 68Gd Naval Postgraduate School Monterey, CA 93943	3
7.	Professor T.P. Stanton, Code 63Sm Naval Postgraduate School Monterey, CA 93943	1
8.	Director Naval Oceanography Division Naval Observatory 34th and Massachusetts Ave. NW Washington, D.C. 20390	1
9.	Commander Naval Oceanography Command NSTL Station Bay St. Louis, MS 39522	1
10.	Commanding Officer Naval Oceanographic Office NSTL Station Bay St. Louis, MS 39522	1
11.	Commanding Officer Fleet Numerical Oceanography Center Monterey, CA 93940	1
12.	Commanding Officer Naval Ocean Research and Development Activity NSTL Station Bay St. Louis, MS 39522	1
13.	Commanding Officer Naval Environmental Prediction Research Facility Monterey, CA 93940	1

14. Chairman Oceanography Department — 1
U.S. Naval Academy
Annapolis, MD 21402

15. Chief of Naval Research — 1
800 N. Quincy Street
Arlington, VA 22217

16. Dr. T.W. Spence (Code 422Po) — 1
Office of Naval Research
Arlington, VA 22217

17. Office of Naval Research (Code 480) — 1
Naval Oceanography Research and Development Activity
NSTL Station
Bay St. Louis, MS 39522

18. Scientific Liason Office — 1
Office of Naval Research
Scripps Institute of Oceanography
La Jolla, CA 92037

19. Commanding Officer — 1
Attn: LT H. Rosner
Naval Polar Oceanography Center
4301 Suitland Road
Washington, D.C. 20390

212947

Thesis
R7719 Rosner
c.1 Evaluation of surface exchange coefficients from MILDEX ocean/atmospheric mixed layer data.